

CONFIDENTIAL

UNOCAL 76

JUL 20 1990

June 20, 1990

JENS PEDERSEN

CONFIDENTIAL

JUL 23 1990

TO: Jens R. Pedersen
David Sussman

FM: Gregg A. Nordquist *GAM*
Randolph C. Thompson *RCT*

RE: INTEGRATED GEOPHYSICAL AND GEOLOGICAL INTERPRETATION OF THE
GLASS MOUNTAIN PROSPECT, CALIFORNIA

TABLE OF CONTENTS

PAGE

Summary and Conclusions.....	1
Recommendations.....	2
Introduction.....	3
Geologic Setting.....	4
Geoelectric Structure.....	8
Temperature and Alteration Distribution.....	13
Fluid Chemistry.....	17
Discussion.....	19
References.....	24
List of Figures and Plates.....	25
Appendix I: Gravity Modeling.....	27
Appendix II: 87-13 X-Ray Diffraction Results.....	28
Appendix III: Chemical Analyses from Flow Tests.....	38

SUMMARY AND CONCLUSIONS

Three primary target areas for deep exploration drilling have been identified in the Glass Mountain Federal Unit. The targets represent three distinct conductance anomalies identified by magnetotellurics (MT) and time-domain electromagnetics (TDEM). The association of the anomalies with high temperatures and shallow, intense alteration leads us to interpret them as three separate upwellings of hot fluids. The three anomalies are apparently localized by zones of enhanced fracture permeability along NE trending structures. The primary heat source for the area appears to be in the vicinity of Glass Mountain.

Three production wells confirm that the large Eastern Conductance Anomaly, which encompasses about 4400 acres, represents a currently active geothermal system. Fluid entries have been encountered at depths ranging from 2600 to 5700 feet and temperatures from 475°F to 514°F. The area exhibits a well-developed vertical zonation of alteration assemblages in general equilibrium with the current temperature regime. A deep exploration well drilled nearby but outside the conductance anomaly was less altered and failed to find production. The reservoir penetrated by well 87-13, near the

V. J. ...

southwestern end of the Eastern Anomaly, appears to be the most promising for commercial production. The well encountered the shallowest production and highest permeability of the four production test wells drilled to date. It also encountered the most intensely altered rocks of any well. However, reservoir fluids from 87-13 appear to have significantly less chloride than the other wells, suggesting the well may not have encountered an upflow zone. Long-term flow testing of a deep well near 87-13 is necessary to evaluate the full significance of the fluid chemistry.

Fluid entries at temperature reversals in two of the production wells indicate that relatively cool water is locally flowing into hotter rock. Although measured fluid entry temperatures are as high as 514°F, chemical geothermometry suggests a source temperature of about 485°F for fluids feeding the three production wells. Lateral flow of 485°F reservoir fluid into hotter, conductively heated rock may account for the observed temperature reversals at fluid entry points. An alternative explanation is that the reservoir is connected to relatively cool, overlying groundwater. In this case, cool water may downflow into the reservoir during long-term production and severely limit the development potential of the area.

The Southwest and Western Conductance Anomalies constitute secondary target areas and encompass about 1650 and 1100 acres, respectively. The anomalies have yet to be tested with deep wells, although shallow temperature gradient holes indicate they are characterized by relatively high temperatures and shallow clay alteration.

RECOMMENDATIONS

Specific recommendations for the large Eastern Conductance Anomaly and the smaller Southwest and Western Anomalies are outlined below. Proposed drill sites are shown in Plate 4 and Figure 20.

1) EASTERN ANOMALY

- a) Drill a deep well in the vicinity of 87-13 to a depth of at least 5000 feet (site 87a-13). There is a high potential that this well will encounter commercial production and help discern between various proposed reservoir models.
- b) After drilling a deep well near 87-13, monitor fluid chemistry and measure interference during long-term flow testing. This will help us infer bulk reservoir properties and the likelihood of cool water downflow.
- c) If the proposed deep well is successful, drill a 3000-foot gradient well south of 87-13 (site 75-24). This well will test the intersection of the conductance anomaly with the southern volcanic rim, a region of very high conductance values (>200 mho). The intersection may localize enhanced fracture permeabilities and relatively shallow circulation of hot water.

d) Drill a deep well near the Hot Spot (site 21-4) at the intersection of the conductance anomaly with the northern volcanic rim. This well will test the possibility of high temperature upflow near Glass Mountain.

2) SOUTHWEST ANOMALY

a) Drill a 4500-foot temperature gradient well at site 71-20. This well will test the heart of the conductance anomaly. If reservoir temperatures are encountered, drill a production test well at some future date.

3) WESTERN ANOMALY

a) Drill a 4500-foot temperature gradient well at the intersection of the conductance anomaly with the inferred ring fracture (site 88-32). Most of this anomaly is not on Unocal leases, so a well should not be drilled until the other anomalies are fully evaluated.

INTRODUCTION

During the past decade the Glass Mountain prospect area has been the focus of intensive exploration efforts by Unocal and other companies. This work has included 24 temperature gradient wells (Figure 1) and extensive geophysical surveys. Since 1984 four production test wells have been drilled in the prospect area (Figure 1).

Pertinent data from the wells are summarized in Table 1. Three of the wells have been successfully produced and are located within a NE trending high conductance (low resistivity) anomaly. Fluid entries range in depth from 2600 feet to 5700 feet and entry temperatures range from 475°F to 514°F. However, steam flow rates range from only 44,000 to 61,000

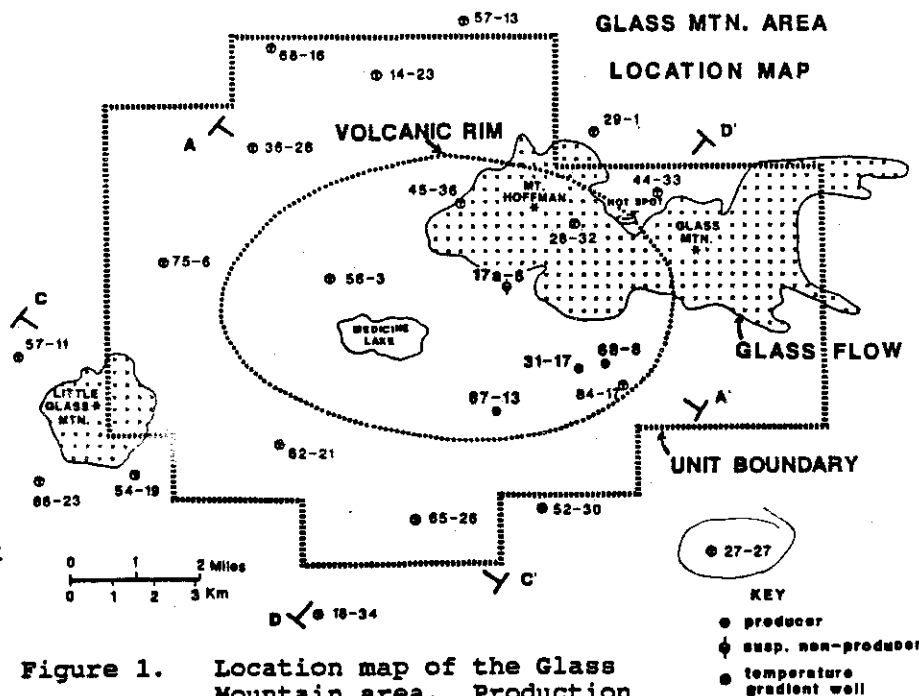


Figure 1. Location map of the Glass Mountain area. Production and temperature gradient wells shown as well as geologic and temperature cross section lines (Figures 2 and 15).

pounds per hour. The shallowest production and best permeability to date was encountered in the slimhole 87-13, the southwesternmost of the three production wells. Although the potential for a viable geothermal resource is good, higher productivity wells are probably necessary for a commercial project.

In 1989, 49 magnetotelluric (MT) sites were measured for improved coverage over the resistivity anomalies. This report integrates these data with 56 MT stations from previous surveys and more than 250 time-domain electromagnetic (TDEM) stations. The resulting geoelectric structure is integrated with drillhole lithology, temperature, and geochemical data to formulate a conceptual model for the Glass Mountain hydrothermal system. The model is used to identify the most likely target areas for commercial production.

Table 1. Production Test Well Data

<u>Well</u>	<u>Total Depth</u>	<u>Prod. Csg. Size</u>	<u>T-max</u>	<u>Entry Depth</u>	<u>Entry Temp</u>	<u>Flow(kph)¹</u>	<u>kh</u>
						<u>TMF</u>	<u>Steam (md. ft.)</u>
87-13	3010'	7"					
31-17	8787'	9 5/8"					
68-8	8417'	9 5/8"					
17A-6	9620'	9 5/8"					

CONFIDENTIAL

Redac

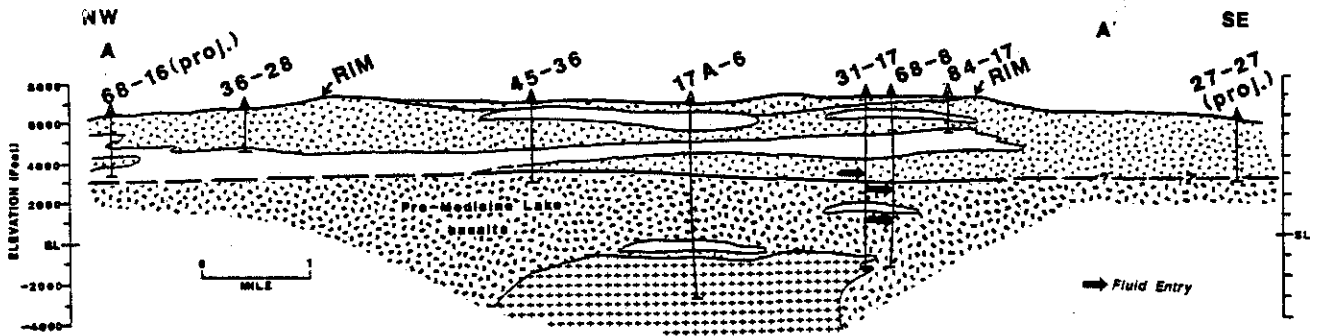
GEOLOGIC SETTING

Volcanology

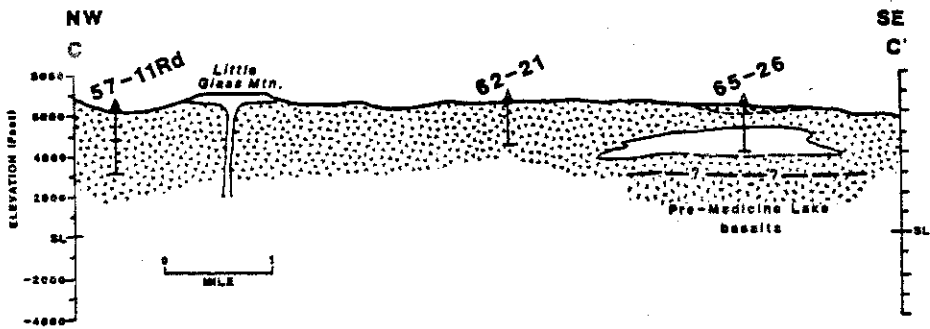
The Glass Mountain prospect is located at the Medicine Lake Quaternary shield volcano near the southern end of the Cascade Range. The volcano is in the Modoc Plateau, slightly east of the main Cascade arc. Medicine Lake is the largest of the Cascade volcanos with lavas covering about 780 square miles and a total volume of about 145 cubic miles (Donnelly-Nolan, 1988). The volcano has about 4,000 feet of relief with an approximately 4 x 6.5 mile elliptical basin at its summit. Defining the basin is a series of volcanic centers that have coalesced to form a constructional rim (Figure 1).

The Medicine Lake Volcano is built on voluminous high-alumina basalts which form the primary rock type of the Modoc Plateau. Pre-Medicine Lake volcanic rocks are divided into two groups: the Warner Basalts, and basaltic to andesitic rocks of the Cedarville series. The Warner Basalts have been dated at 1 m.y. (Thompson, 1981) and the Cedarville series is of Miocene age (Anderson, 1941). These older rocks are overlain by varied mafic to silicic lavas and minor tuffs related to the Medicine Lake Volcano (Figure 2). The pre-Medicine Lake basalts can be distinguished by their relatively

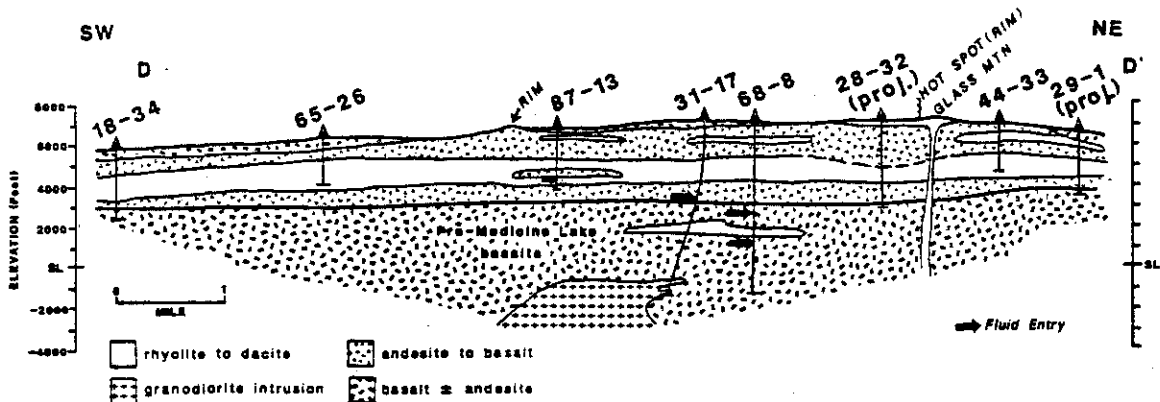
GEOLOGIC CROSS SECTIONS



2)
Medicine Lake Volcano
X-Section



b)



c)

rhyolite to dacite	andesite to basalt
granodiorite intrusion	basalt ± andesite

Figure 2. Geologic cross sections through the Medicine Lake Volcano. a) NW-SE section across the summit basin, b) NW-SE section SW of the summit basin, c) SW-NE section across the summit basin. Location of section lines shown in Figure 1.

homogenous composition, lower alkali content and typically porphyritic texture. The most recent Medicine Lake lavas are Holocene bimodal basalt and rhyolite. The youngest and largest silicic center is the 1000 year old Glass Mountain, with an extruded volume of about 0.24 cubic miles.

Deep drilling has confirmed the presence of a cooled intrusion which had been interpreted from gravity data to exist beneath the volcano (Figure 3 and Appendix I). The well 17a-6 intersected a granodiorite intrusion at a depth of about 8000 feet and remained in it to the T.D. of 9620 feet. Well 31-17 encountered a stringer or sill of granodiorite at about the same depth. A contact preserved in a core obtained from the well 31-17 suggests that the

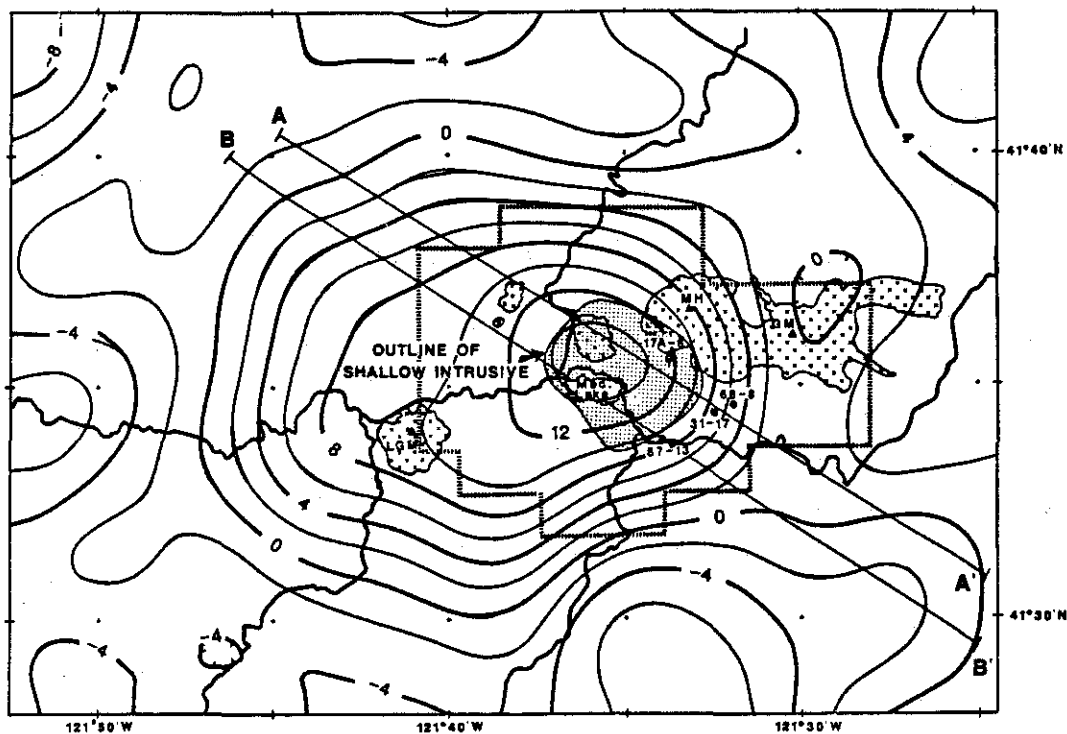


Figure 3. Residual Bouguer gravity contours and outline of shallow intrusive body. Regional gravity effect removed using a high pass filter. Shallow intrusion (shaded) determined with 2 1/2-D interpretations and is at a depth of about 8000 feet. Also shown are locations for 2 1/2-D gravity interpretations (Figure 1a).

granodiorite intruded the pre-Medicine Lake basalts. It is likely that the intrusion was a source magma for some of the Medicine Lake lavas. Geophysical studies have not detected a large, still-molten body beneath the volcano (Evans and Zucca, 1988). However, it is possible that a magma body (or bodies) too small to detect (<0.7 cubic miles) may underlie the volcano (Donnelly-Nolan, 1988).

Structural Setting

The Medicine Lake Volcano is located at the transition between the Cascade arc to the west and the Basin and Range province to the east. North and NW trending Basin and Range normal faults project toward the volcano and are buried beneath it. The Medicine Lake Volcano is located at the intersection of the Basin and Range structures and a strong ENE volcanic trend extending from Mount Shasta, which is about 35 miles to the west. Donnelly-Nolan (1988) has interpreted Medicine Lake's position behind the crest of the Cascades as a back-arc, extensional environment.

The distribution of vents surrounding the summit basin of the Medicine Lake volcano suggests a zone of enhanced permeability, possibly along now-buried ring fractures. Donnelly-Nolan (1988) and Anderson (1941) have interpreted the basin as a caldera collapse feature. However, no significant offset is evident in the subsurface across the volcanic rim (Figure 2) and there are only minor accumulations of tuff. Despite the lack of evidence for major caldera collapse, the elliptical distribution of volcanic vents around the shallow intrusion could indicate a causal relationship, possibly incipient caldera collapse.

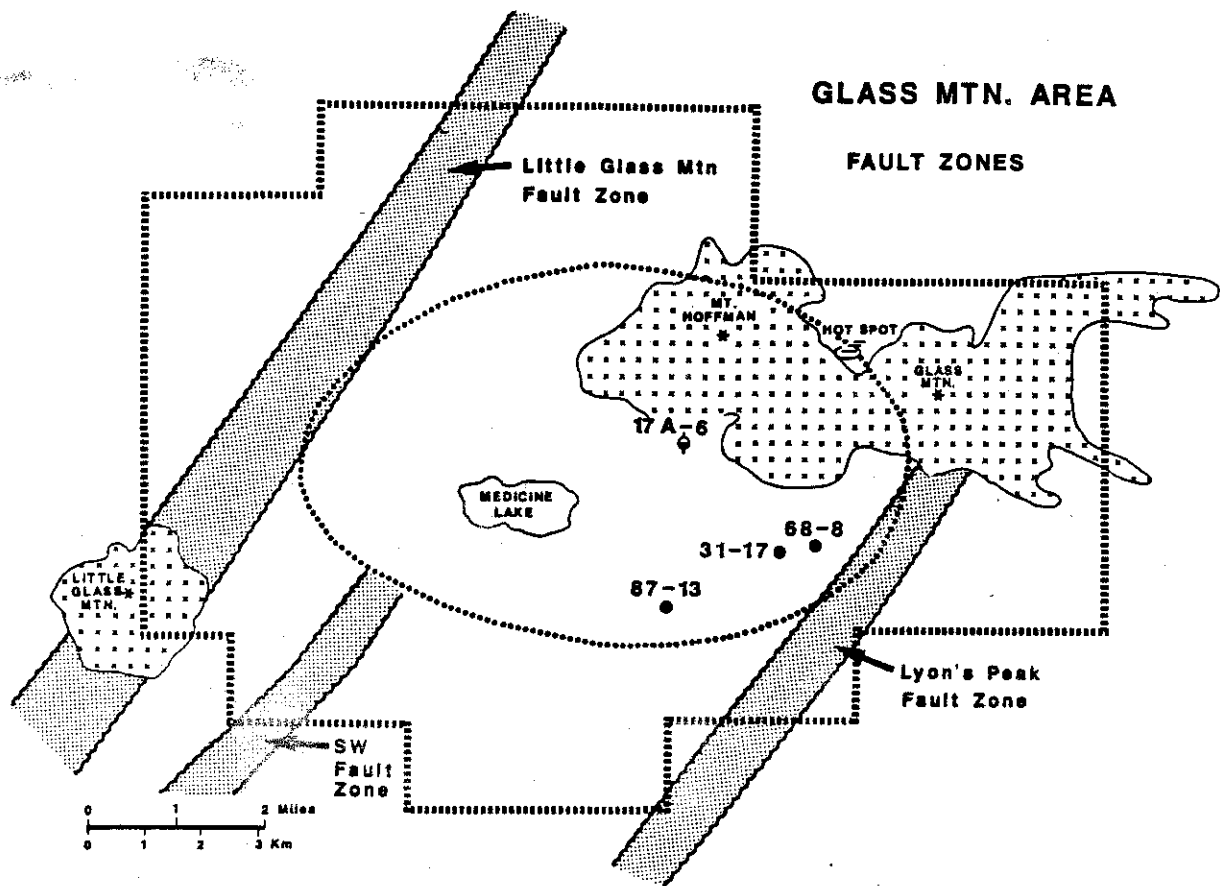


Figure 4. Location of major fault zones.

The youngest faults affecting the Medicine Lake lavas are NE trending structures which form three major fault zones. The most prominent structural feature is the Little Glass Mountain Fault Zone (Figure 4), which is marked by glass flows and tensional ground cracks. The Lyon's Peak Fault Zone intersects the eastern volcanic rim and is characterized by ground cracks and numerous explosion craters. The Southwest Fault Zone is expressed by faults with relatively minor ground cracks (McDannel and Bodell, 1985). A burst of seismic activity in late 1988 to mid 1989 in the vicinity of the Medicine Lake Glass Flow (Figure 5) had a tectonic origin (Steve Walter, USGS, pers. comm.) but did not correlate with any known faults.

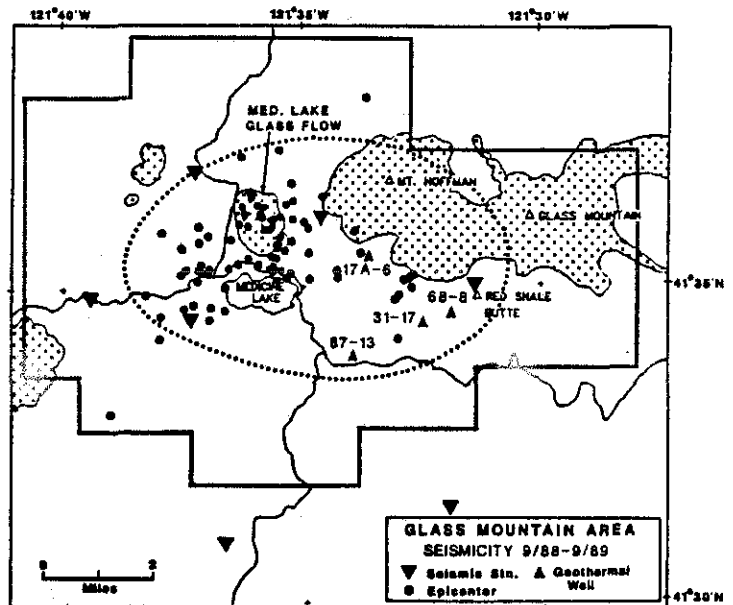


Figure 5. Earthquake epicenter locations, September 1988 - September 1989 (USGS data). Shows events with magnitude >0.5.

MT Interpret X-Section

GEOELECTRIC STRUCTURE

Resistivity data have delineated three major anomalies at Medicine Lake with thick sections of low resistivity rock. The areas have been identified by integrating shallow and deep resistivity data. The shallow geoelectric structure (<3,000 feet) has been determined using more than 250 TDEM sites measured by Unocal, Occidental Petroleum and the USGS (Plate 1). These data were also used to correct for near-surface static shifts in the deeper sensing MT data, which include 105 sites from four Unocal surveys (Plate 2). Interpretation of the geoelectric structure was done using Bostick inversions of the MT's invariant apparent resistivity and phase data, and Bostick conversions of one-dimensional (1-D) TDEM resistivity models (Stark, 1985). Bostick resistivities smooth the resistivity structure with depth and make it easier to visualize and correlate the geoelectric structure between MT and TDEM stations. However, by virtue of the smoothing, vertical and lateral boundaries are not well-resolved. For this reason, a two-dimensional (2-D) MT resistivity model was also constructed to better define vertical and lateral boundaries.

The geoelectric structure of the Medicine Lake volcano in cross section is characterized by zones of low resistivity which are sandwiched between layers of higher resistivity. This is illustrated in Figure 6 which shows a 2-D resistivity structure derived from the MT data. The figure also shows how the geoelectric

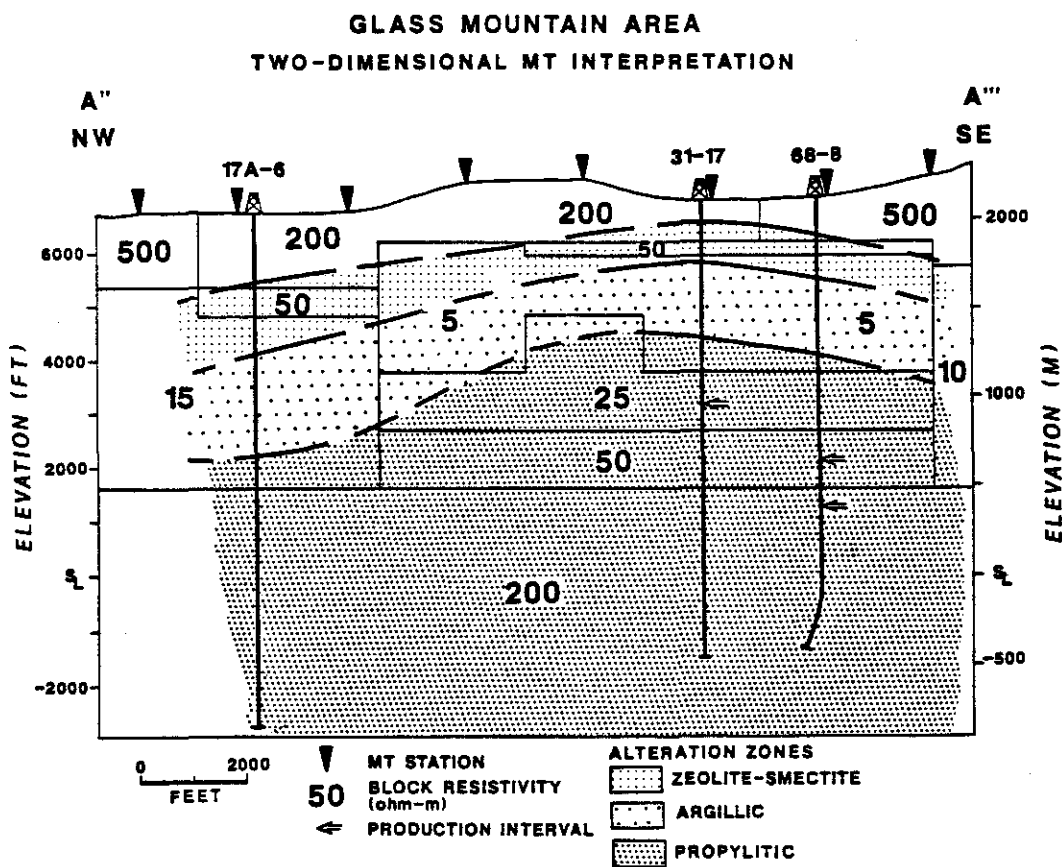


Figure 6. Two-dimensional MT interpretation with alteration zonation. Location of section shown in Figure 9.

structure relates to downhole alteration mineralogy in the wells 31-17, 68-8 and 17a-6. The high surface resistivities (200-500 ohm-m) correlate with unaltered volcanic rocks, which are very poor electrical conductors. The low resistivities (5 and 15 ohm-m) of the middle layer correspond with alteration zones rich in clay (smectite-zeolite to argillic alteration). The low resistivities of this layer are due primarily to high ion exchange capacities of the clays, but may also be enhanced by water saturation and higher rock porosities. The deep layer with relatively high resistivities correlates with the propylitic alteration zone (25-50 ohm-m at 31-17 and 68-8). The higher resistivities are probably due to lower ion exchange capacities for this grade of alteration. Higher resistivities at 17a-6 in the argillic (15 ohm-m) and propylitic (200 ohm-m) alteration zones correspond to relatively less intense alteration in the well (Carrier, 1989a).

The TDEM data at a depth of 1500 feet below the surface delineate three NE trending anomalies with resistivities less than 10 ohm-m (Figure 7 and Plate 1). The anomalies are located along the eastern and western volcanic rim and along a SW trend from Medicine Lake. Drilling data indicate that the eastern anomaly corresponds to a region with clay alteration at less than 1000 feet drilled depth. Regions of higher resistivity correlate with areas where clay alteration is first encountered at deeper levels (Nordquist, 1986; Carrier, 1987).

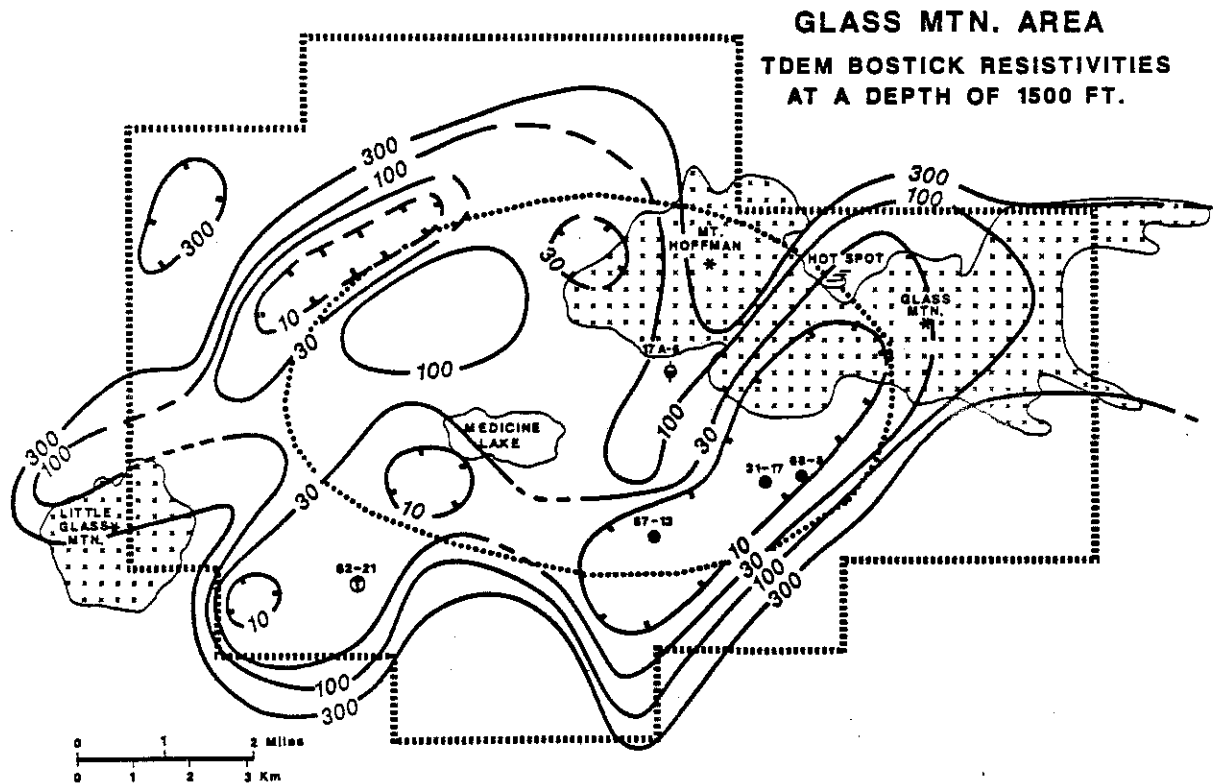


Figure 7. Contour map of TDEM Bostick resistivities at 1,500 feet depth. Station locations shown in Plate 1.

At a depth of 5,000 feet below the surface the geoelectric structure is dominated by a resistivity high encompassing the western half of the Medicine Lake summit basin (Figure 8 and Plate 2). Resistivities of less than 20 ohm-m are located near the eastern margin of the summit basin and cut across a NE-SW trending ridge of greater than 20 ohm-m. The broad areas of less than 10 and 20 ohm-m on the southern and northern flanks of the volcano, respectively, are related to a regional low resistivity layer. This layer is observed in other parts of the Cascades and is not a viable drilling target.

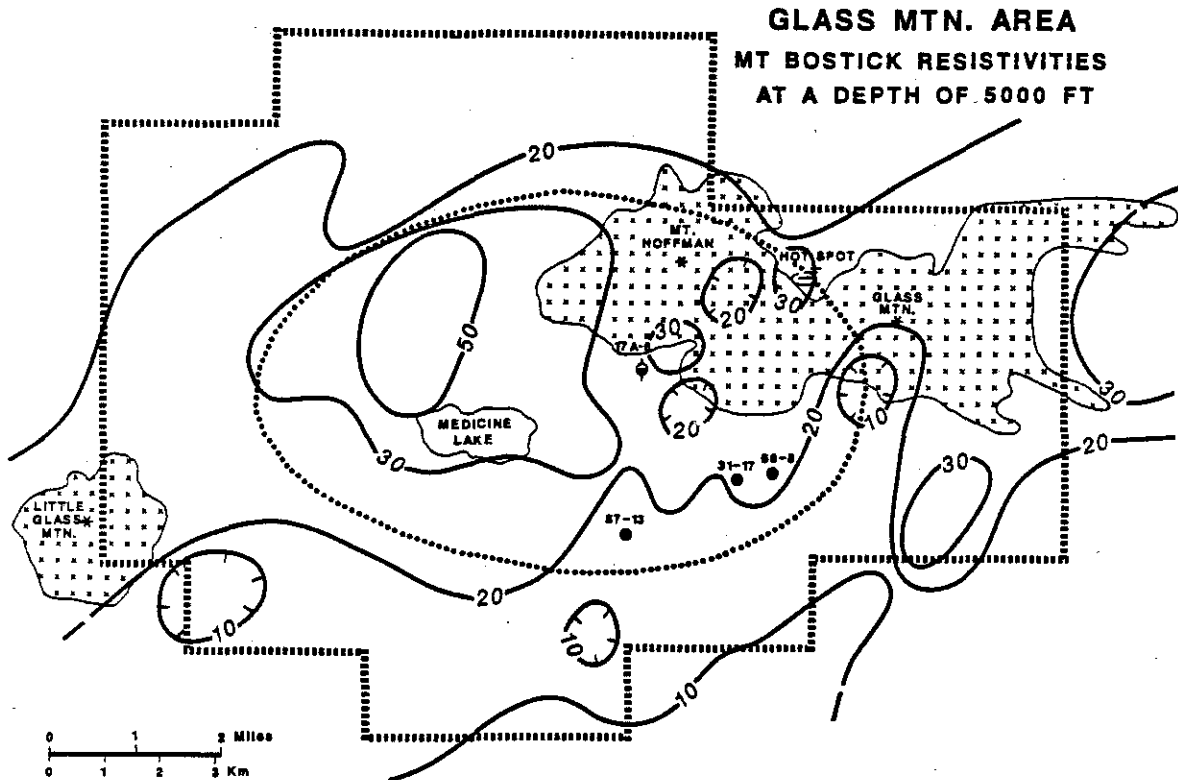


Figure 8. Contour map of MT Bostick resistivities at 5,000 feet depth. Station locations shown in Plate 2.

Integration of the shallow and deep geoelectric structure to a depth of 5,000 feet outlines three major conductance anomalies (Figure 9 and Plate 3). The conductance is determined from the MT Bostick resistivity models by taking the product of the conductivity ($1/\text{resistivity}$) and the thickness of a layer with that conductivity. Because the conductance is inversely related to resistivity, high values outline areas with thick sections of anomalously low resistivities. The three conductance anomalies are coincident with the shallow TDEM low resistivity anomalies (Figure 7), indicating the shallow and deep low resistivities are vertically continuous. The largest conductance anomaly trends NE and is located in the eastern part of the basin

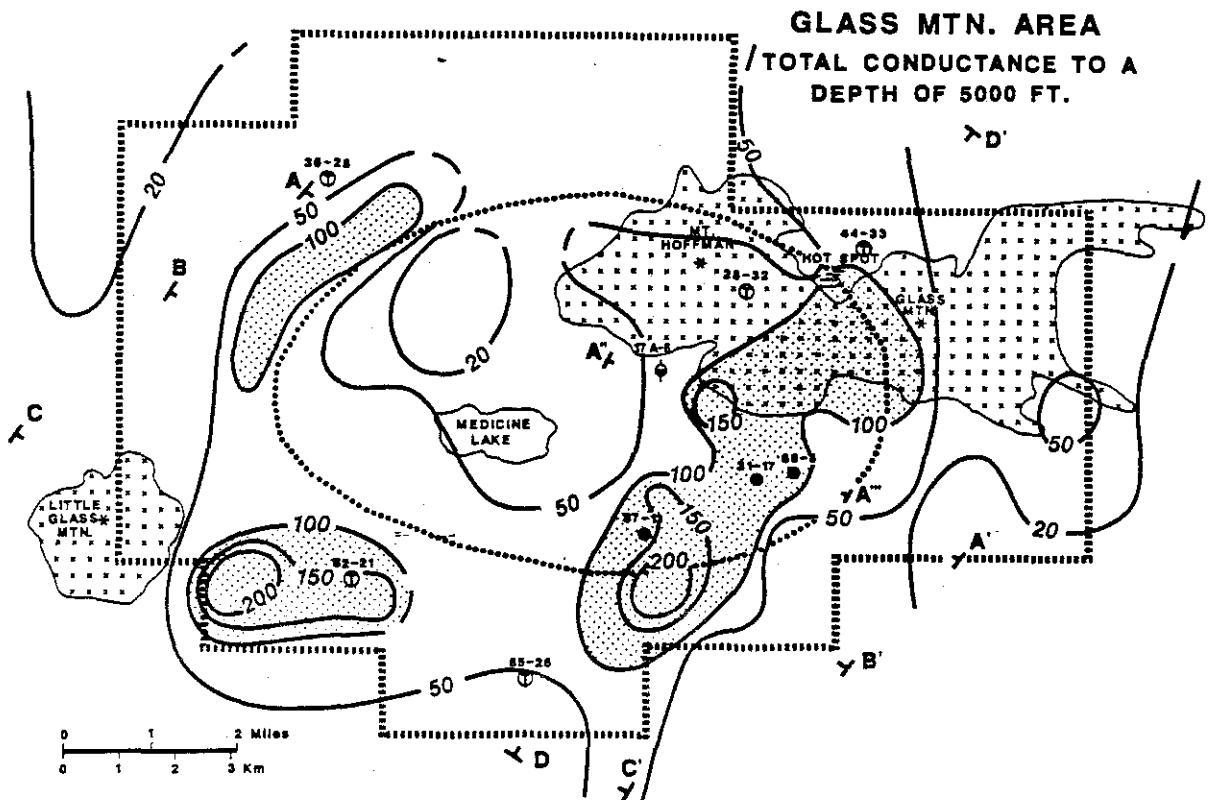


Figure 9. Total conductance integrated to a depth of 5,000 feet. Shaded areas denote areas with conductances of >100 mho. Also shown are locations for geoelectric cross sections (Figures 11 and 12). Station locations shown in Plate 3.

abutting the volcanic rim. This Eastern Anomaly, which parallels the Lyon's Peak Fault Zone (Figure 10), encompasses about 4400 acres and contains all three productive wells drilled to date at Glass Mountain. The Southwest Anomaly encompasses about 1650 acres near the intersection of the SW Fault Zone with the volcanic rim. The narrow NE trending Western Anomaly is at the intersection of the Little Glass

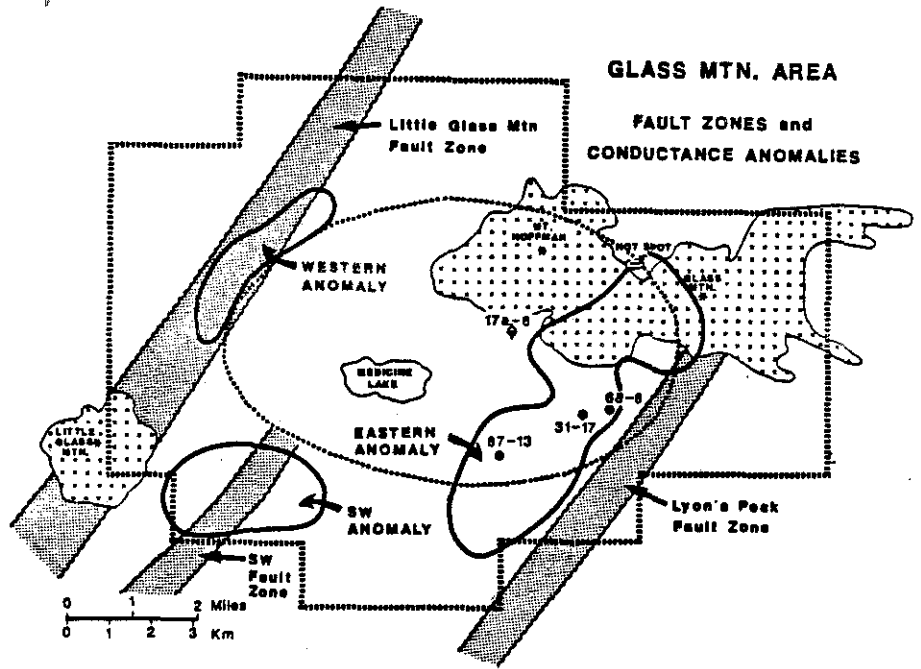


Figure 10. Location of major fault zones and conductance anomalies.

Mountain Fault Zone with the volcanic rim and encompasses about 1100 acres. Areas with unusually high conductance (>150 mho) are found in the Southwest Anomaly and in the Eastern Anomaly near 87-13 and NW of 31-17. These high conductances correspond to areas with subsurface resistivities of less than 5 ohm-m.

Geoelectric cross sections suggest that the three major conductance anomalies are separate. The separation of anomalies is most easily seen by the confinement of the 10 ohm-m layer in sections A-A' and B-B' to the distinct Eastern and Western Anomalies (Figure 11). Section C-C' across the Southwest Conductance Anomaly also suggests that it is a distinct feature not directly connected to the other anomalies (Figure 12). In the Eastern Anomaly, the 10 ohm-m layer extends at shallow levels almost continuously from southwest of 87-13 to the Hot Spot, a distance of about five miles (section line D-D', Figure 12). At the SW and NE ends of the line the high resistivity cover gets thicker and the low resistivity layer deepens. Production from 31-17 and 68-8 are from below the 10 ohm-m zone (Line A-A') while production in 87-13 (Line B-B') is within the 10 ohm-m layer.

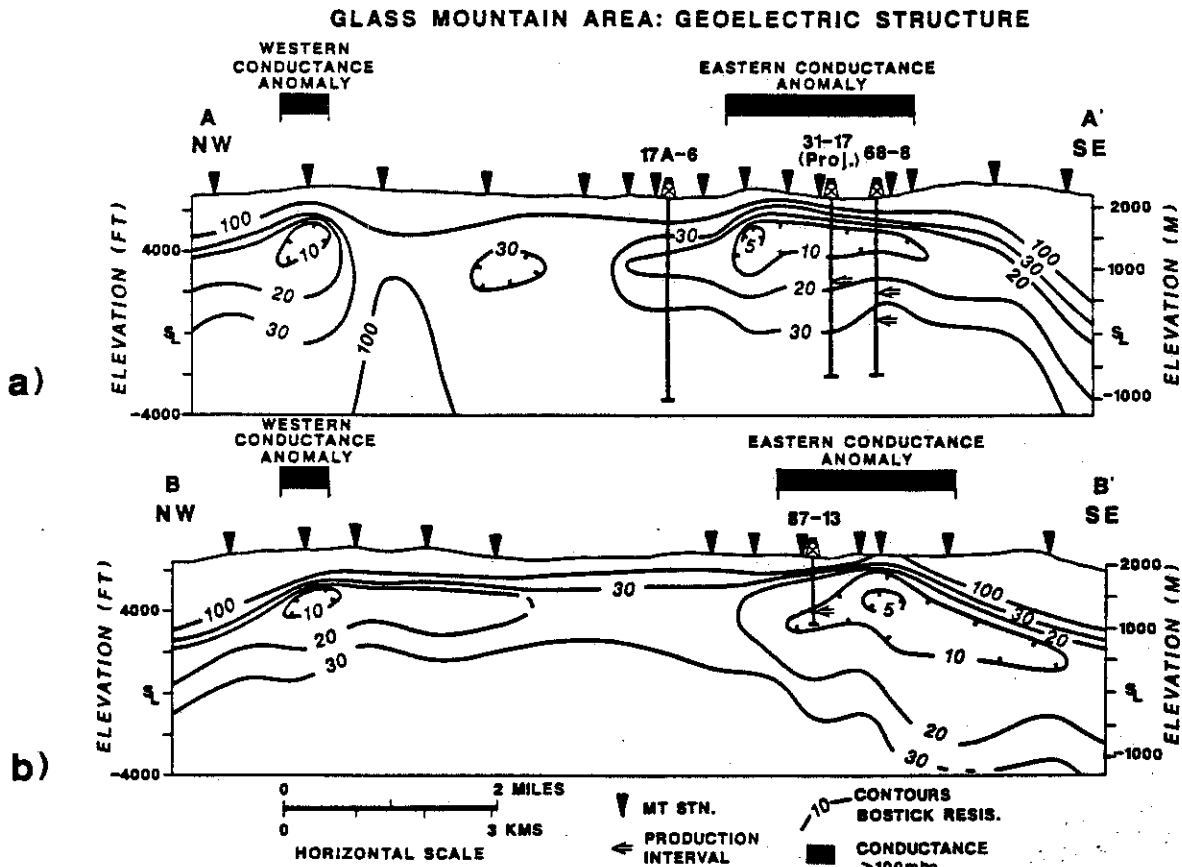


Figure 11. Geoelectric cross sections with contoured Bostick resistivities, Lines A-A' and B-B'. a) NW-SE section north of Medicine Lake, through Western and Eastern Conductance Anomalies, b) NW-SE section through Medicine Lake. Location of section lines shown in Figure 9.

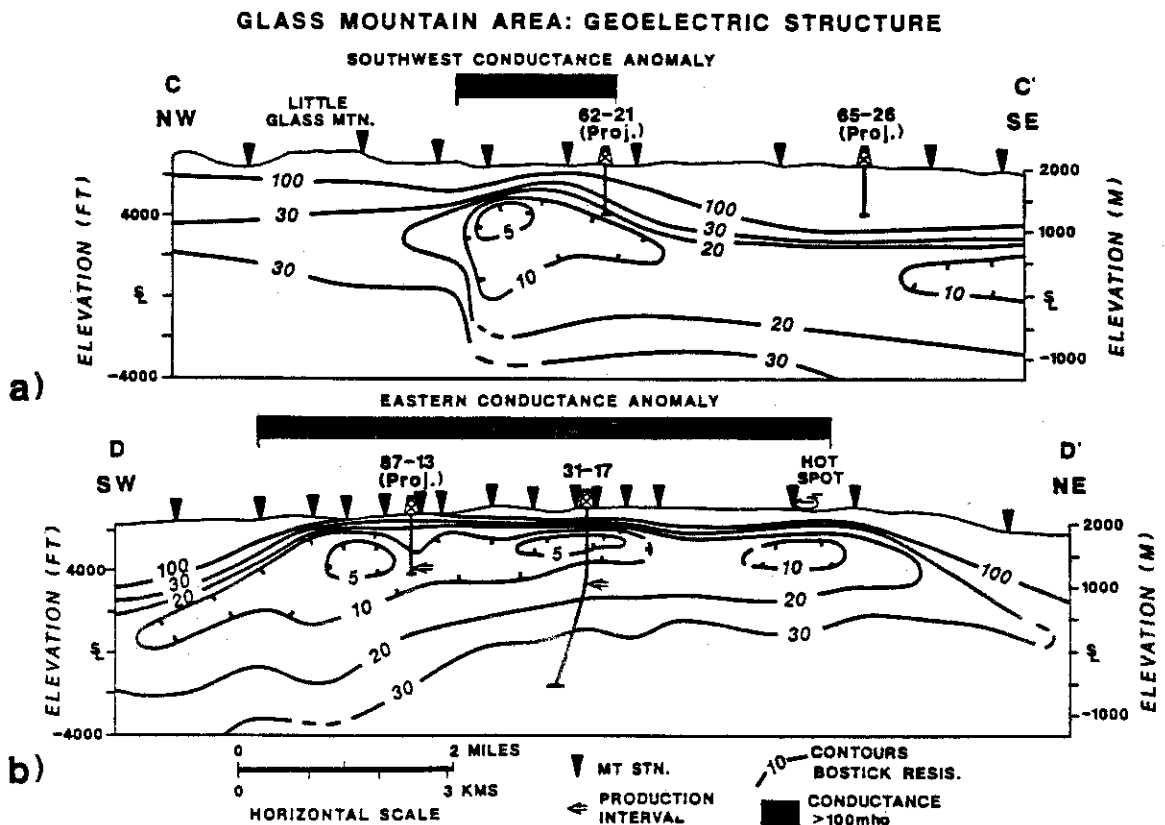
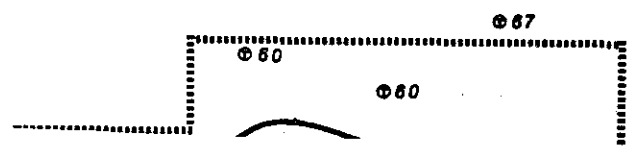


Figure 12. Goelectric cross-sections with contoured Bostick resistivities, Lines C-C' and D-D'. a) NW-SE section through SW Anomaly, b) SW-NE section through Eastern Conductance Anomaly. Location of section lines shown in Figure 9.

TEMPERATURE AND ALTERATION DISTRIBUTION

A region of shallow high temperatures ($>450^{\circ}\text{F}$) has been identified at the summit of the Medicine Lake Volcano, centered near the eastern and southern volcanic rim. Data from 24 temperature gradient wells and four production test wells have been used to estimate temperatures at depths of 2000 and 3000 feet below the surface (Figures 13 and 14, respectively). The regions of shallow elevated temperatures at both levels correlate with the major conductance anomalies. The concurrence of relatively high temperatures and shallow alteration with the three conductance anomalies can also be seen in cross section (Figure 15).

The highest temperatures and best developed alteration presently observed are in the Eastern Conductance Anomaly. Temperatures of at least 490°F exist at depth throughout the anomaly with a significant region greater than 530°F near Glass Mountain (Figure 15c). A well-developed vertical zonation of alteration minerals described by Carrier (1987, 1989a) can be correlated with the high subsurface temperatures. A zeolite-smectite zone generally occurs at temperatures ranging from 150°F to 300°F . Recorded temperatures in the argillic zone range from about



GLASS MTN. AREA
TEMPERATURE CONTOURS
AT 2000'

Redact

CONFIDENTIAL

0 1 2 3 4 5 6 7 8 9

670

Figure 14. Interpreted temperature contours at 3,000 feet depth.

TEMPERATURE AND ALTERATION CROSS SECTIONS

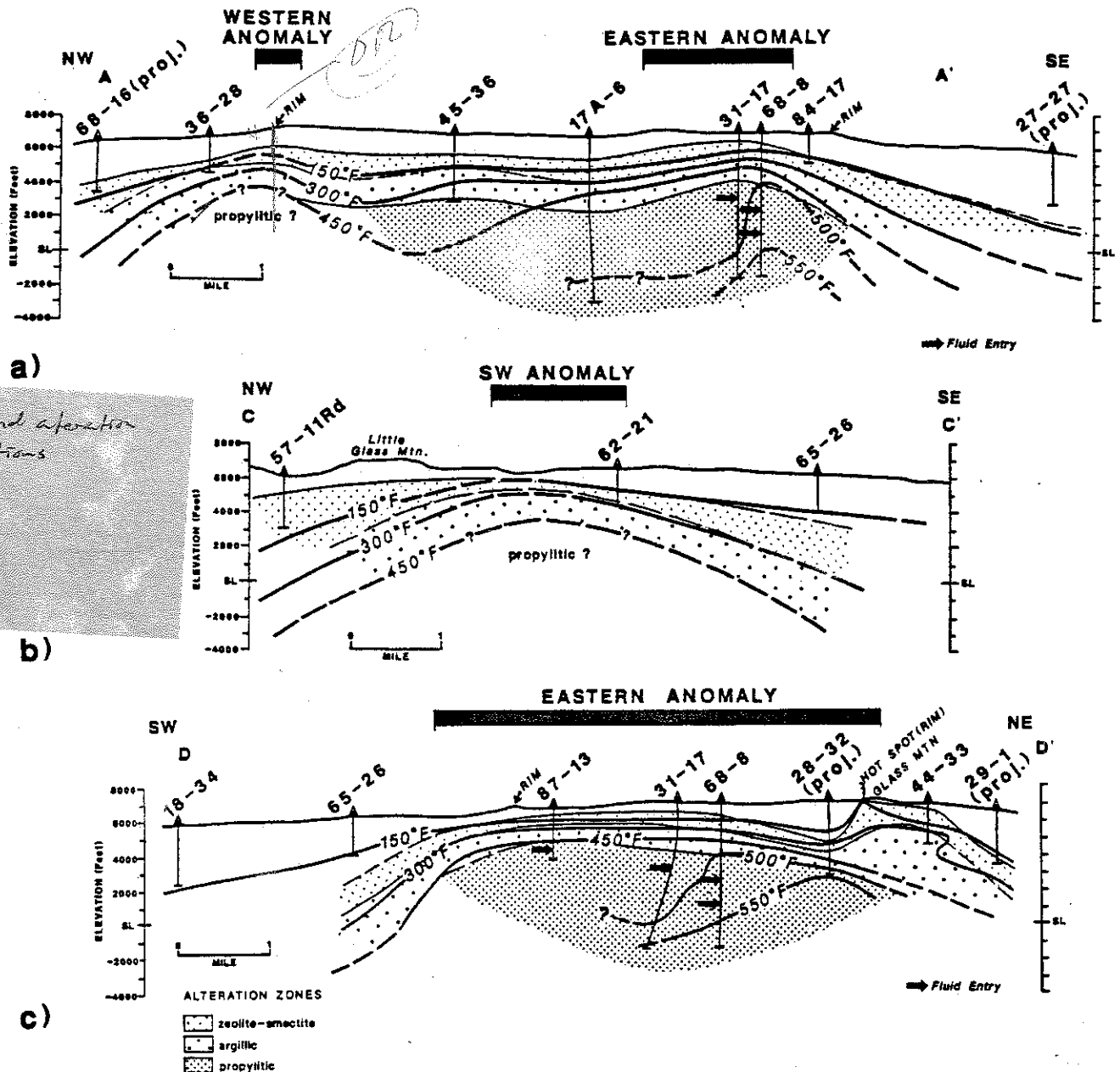


Figure 15. Temperature and alteration cross sections through the Medicine Lake Volcano. a) NW-SE section through the Western and Eastern Conductance Anomalies, b) NW-SE section through the Southwest Anomaly, c) SW-NW section through the Eastern Anomaly. Location of section lines shown in Figure 1.

300°F to 450°F, and propylitic alteration is generally restricted to regions with measured temperatures greater than 450°F. All fluid entries in the exploration wells are restricted to the propylitic alteration zone, which is characterized by chlorite and epidote.

The shallowest and most intensely developed alteration is observed in the 87-13 well. Propylitic alteration with epidote is present as shallow as 1300 feet and is pervasive below 2000 feet. This is the only Glass Mountain well to exhibit potassium feldspar flooding (below 2300 feet), which is often correlated

with high temperature upflow in ore deposits (Lutz, pers. comm.). It is also the only well to contain common veins of prehnite, which are present in the potassium feldspar alteration zone (see Appendix II for complete x-ray diffraction results).

Temperature profiles indicate that fluid entries in 31-17 and 68-8 are locally associated with temperature reversals (Figure 16). Fluid entry temperatures range from a low of 475°F in 31-17 to a high of at least 514°F in 68-8. In 31-17 the single entry at 3800 feet occurs at the temperature minimum of a 14°F reversal. No completely stable temperature profile has yet been obtained from 68-8, but it appears that the entries also occur at a small temperature reversal. A stable temperature profile has also not yet been obtained from 87-13, although the fluid entry appears to occur at a temperature maximum of 490°F. Due to a bad casing cement job, stable temperatures are not available below a depth of 4550 feet from the apparently unproductive well 17a-6. However, fluid inclusion data suggest a temperature reversal of about 25°F below the casing (Carrier, 1989b).

The Southwest and Western Conductance Anomalies also exhibit elevated temperatures and enhanced alteration. The temperature gradient well 62-21 (TD 2142 feet) was drilled in the eastern part of the Southwest Anomaly. The well had a maximum temperature of 311°F with a bottom hole gradient of 8.8°F/100 feet and relatively shallow argillic alteration (Figure 15b). The narrow, NE trending Western Conductance Anomaly has not been drilled. However, about one-half mile to the north, the temperature gradient well 36-28 (TD 2146 feet) encountered a bottom hole temperature of 193°F with a high bottom hole gradient

TEMPERATURE vs ELEVATION

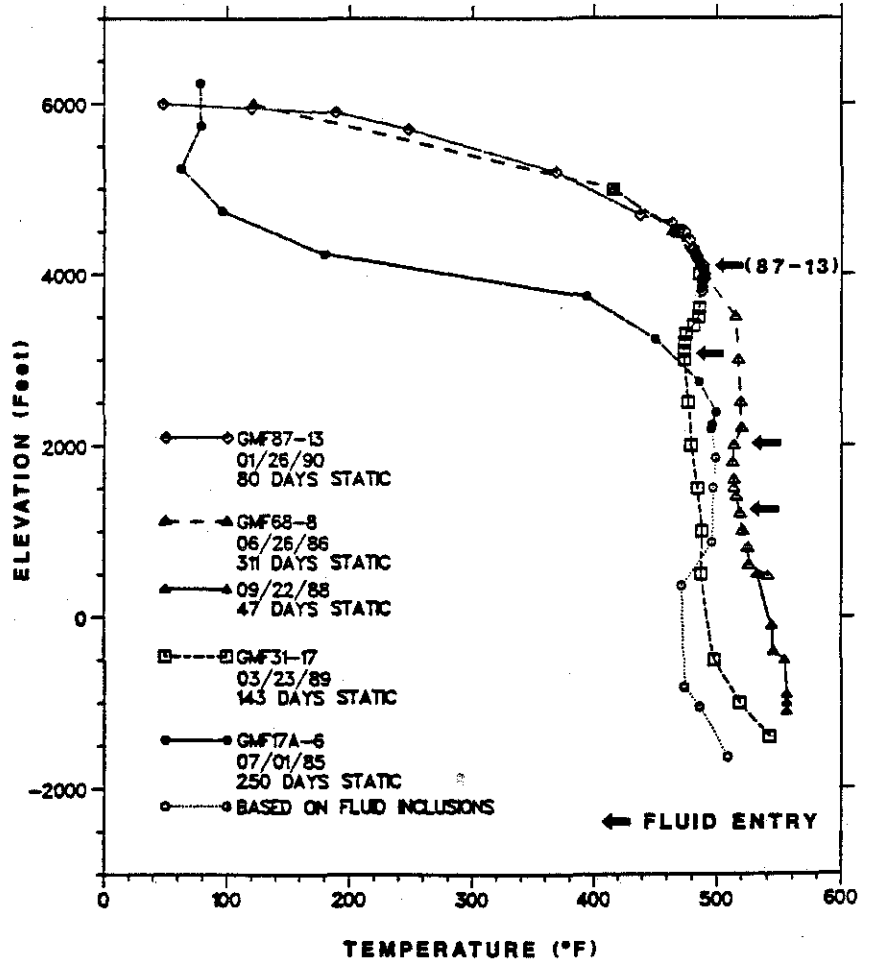


Figure 16. Temperature vs elevation profiles from the wells 17a-16, 31-17, 68-8 and 87-13. Fluid entry points also shown.

(19°F/100 feet) in argillically altered rocks (Figure 15a).

FLUID CHEMISTRY

The reservoir fluids encountered at Glass Mountain are low-gas, dilute NaCl brines that are very benign relative to fluids in other Unocal fields around the world. The total dissolved solids are only about 3000 ppm, about one-half that of Bulalo and almost two orders of magnitude less than the Salton Sea (Figure 17a). Non-condensable gases in the steam average about 0.15 weight percent with only about 50 ppm H₂S. These values are two to twenty times less than at other Unocal fields (Figure 17b).

Completely representative analyses of the Glass Mountain fluids are not yet available because samples collected from the three production wells are still showing signs of contamination from acid jobs or drilling fluids. Acid was injected into 31-17 in 1988 prior to any flow testing, and acid was injected into 68-8 in 1989 prior to its only long test. Although no acid was injected into 87-13, it was flow tested for less than a day. The effect of acid jobs is vividly demonstrated by tracking fluoride, which is partially derived from injected hydrofluoric acid, in samples collected over time from 31-17 and 68-8 (Figure 18a). Fluoride levels probably most representative of the reservoir are about 1.5 ppm and were collected in 1988 from 68-8 before it was acidized. Fluoride levels in the wells at the end of testing in 1989 were still two to three times higher than the inferred base level. This agrees with calculations of the total

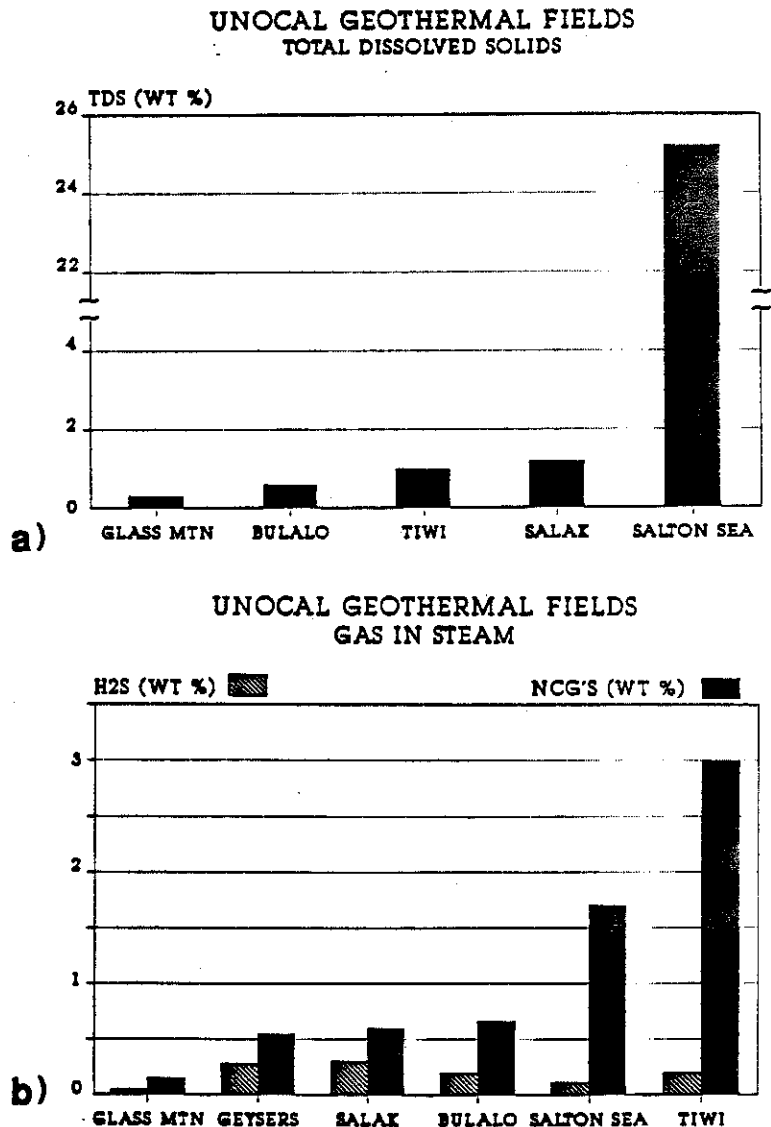


Figure 17. Total dissolved solids (TDS), total gas, and H₂S concentrations in reservoir fluids from Unocal geothermal fields. TDS is flash-corrected. Total gas and H₂S shown as weight % in steam. a) total dissolved solids, b) total gas and H₂S.

fluoride produced, which amounts to only about one-third to one-quarter of the total fluoride injected.

Chloride levels were also affected by the acid jobs due to injected HCl, but appear to have stabilized at about 1400 - 1500 ppm in 31-17 and 68-8 (Figure 18b). By contrast, chloride levels in 87-13 appear to be much lower at about 950 ppm. However, the chemistry of this well had not yet stabilized.

Chemical geothermometry yields values of about 480°F to 485°F for the Glass Mountain reservoir fluids. Calculated Na-K-Ca geothermometry temperatures stabilize at about 485°F for 68-8 and 87-13 and at about 480°F for 31-17 (Figure 19a). Quartz conductive geothermometry was strongly affected by excess silica introduced during the acid jobs. However, values for 31-17 stabilize at about 490°F and pre-acid job values for 68-8 were about 485-495°F at the end of testing in 1988 (Figure 19b). High quartz geothermometry of about 520°F calculated for 87-13 is probably due to high silica contents in flashed 68-8 brine that was injected into the well just prior to flow testing. Chemical analyses from the flow tests are listed in Appendix III.

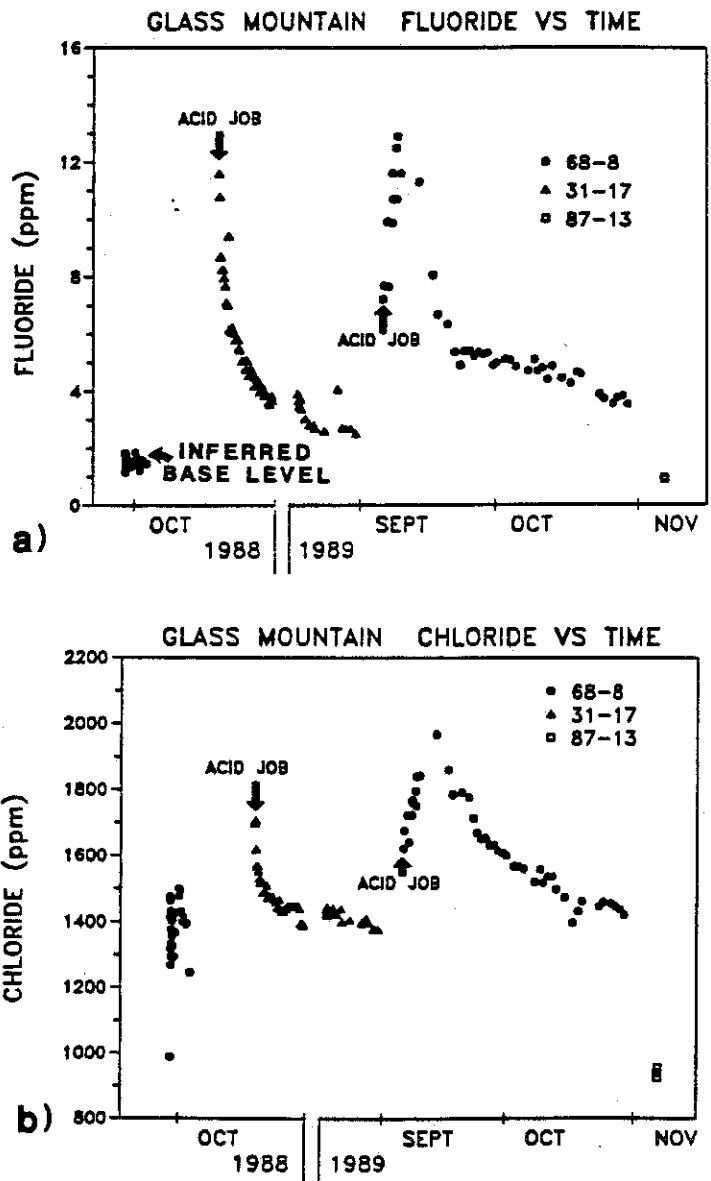


Figure 18. Fluoride and chloride concentrations (flash-corrected) vs time for produced fluids from the Glass Mountain production wells. a) fluoride, b) chloride.

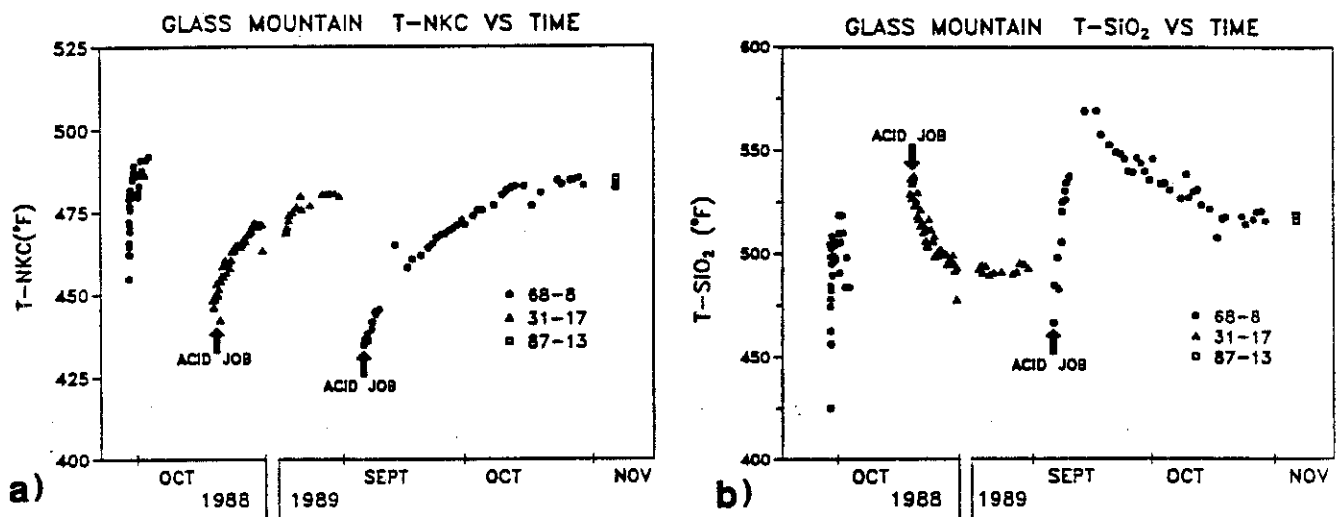


Figure 19. Calculated chemical geothermometers vs time for produced fluids from the Glass Mountain production wells. a) Na-K-Ca, b) quartz conductive.

DISCUSSION

Three major conductance anomalies outline the primary target areas for a commercial geothermal reservoir at Glass Mountain (Figure 10 and Plate 3). The distinct anomalies are interpreted to delineate areas where rocks are intensely altered to clay at relatively shallow depths. The areas of high conductance appear to define the primary flow paths for three separate upwellings of hot fluids. The permeability paths are probably controlled by NE trending fault zones with potentially enhanced permeabilities where the fault zones intersect ring fractures buried beneath the volcanic rim.

The three conductance anomalies are interpreted to delineate areas with good potential for high reservoir temperatures at relatively shallow depths. This is based on temperature gradient hole data which clearly show the close association of elevated temperatures at depths of 2000 and 3000 feet with the anomalies (Figures 13 and 14). This trend is likely to continue to depth. Areas with interpreted temperatures of greater than 450°F at a depth of 4000 feet also correspond with the conductance anomalies (Figure 20 and Plate 4). Recommended drill site locations are shown on these latter two maps.

The primary target area at Glass Mountain is the large Eastern Conductance Anomaly which encompasses about 4400 acres. Three producing wells drilled in the anomaly confirm the presence of a geothermal system. The wells encountered a well-developed vertical zonation of alteration minerals in general equilibrium with the current temperature regime. The well 87-13 had the highest permeability (17,500 millidarcy feet) and produced 44,000 lbs/hour steam from a slimhole completion (see Table 1). Wells drilled outside the anomaly have not produced and exhibit less intense alteration. The principal heat anomaly appears to be centered along the NE trend of the conductance anomaly, with the primary

CONFIDENTIAL

A handwritten signature in cursive script, appearing to read "Redax", is centered on the page below the "CONFIDENTIAL" stamp.

Figure 20. Interpreted temperature contours at 4,000 feet depth. Measured and extrapolated temperatures shown for temperature gradient and production wells. Also shown are five proposed drillhole locations.

heat source in the vicinity of Glass Mountain (Figure 20). Good candidates for enhanced permeabilities occur south of 87-13 and southeast of the Hot Spot where the conductance anomaly intersects the volcanic rim. An additional source of enhanced permeability may be increased fracturing associated with the edge of the granodiorite intrusion (Figure 3).

The Southwest and Western Conductance Anomalies are secondary targets which may represent smaller areas of hot fluid circulation. The Southwest anomaly in particular is large enough (1650 acres) to contain a substantial geothermal resource. High conductances suggest the core of the anomaly is centered about one mile west of 62-21 (Figure 9). We believe there is a good possibility of encountering permeability and temperatures greater than 450°F at depths of less than about 4000 feet in both of these anomalies.

Reservoir Models

Reservoir models have been developed for the large Eastern Conductance Anomaly to delineate areas most likely to contain commercial production. The average steam flow rate from our current wells is about 50,000 pounds an hour (see Table 1), probably insufficient for a major geothermal project. Perhaps an

even more disturbing aspect of the wells drilled to date is the local association of fluid entries with temperature reversals, a very unusual feature in known geothermal fields (Strobel, pers. comm.). This indicates flow of relatively cool water into hotter rock. Reservoir models developed with the aid of the Reservoir Department provide alternate explanations of our current data. The models are referred to as the "Downflow" and "Lateral Flow" models and can help identify areas most likely to contain commercial production.

One reasonable explanation of the association of fluid entries with temperature reversals is that the geothermal system is connected to relatively cool overlying groundwater. Cool groundwater may be entering the reservoir along permeable channels too rapidly to be heated to temperature equilibrium with the surrounding rocks. Intense alteration and fluid inclusion homogenization temperatures indicate previous, higher temperature events at the entries associated with temperature minima in 31-17 and 68-8. This suggests that the current entries have been the major pathways for hot fluid circulation in the past (Carrier, 1989b). It is possible that cooler water is back-flowing into the reservoir along these former avenues of hot water flow. Long-term production may accelerate the influx of cool water, a possibility that would severely limit the development potential of the area. However, two variations of the downflow model suggest possible areas of permeable upflow in the Eastern Conductance Anomaly.

In Downflow Model #1 the shallow, productive entry in 87-13 is interpreted to occur over a region of permeable upflow, probably at temperatures of about 500°F or more (Figure 21). This model is supported by intense alteration at shallow depths in the well and

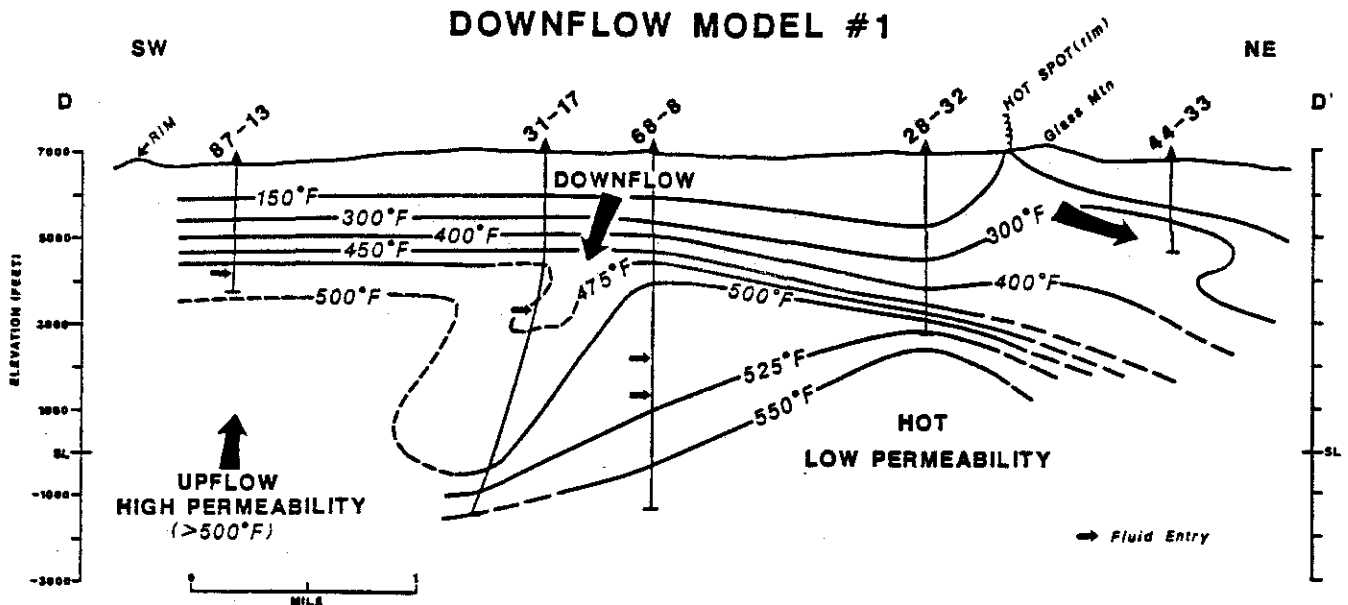


Figure 21. Reservoir downflow model #1 showing upflow near 87-13.

correspondingly high conductances. These features suggest that this region has been the focus of vigorous hydrothermal circulation and may represent a region of high permeability. In this model, the hot region near Glass Mountain is interpreted as a low permeability area based on the conductive gradient observed in the TGH 28-32 and the poor permeability of 68-8.

In Downflow Model #2, potential for hot, permeable upflow is inferred in the undrilled region northeast of 68-8 as well as in the vicinity of 87-13 (Figure 22). Well data strongly suggest that high temperatures exist at depth in the vicinity of the Hot Spot, with probable outflow to the northeast.

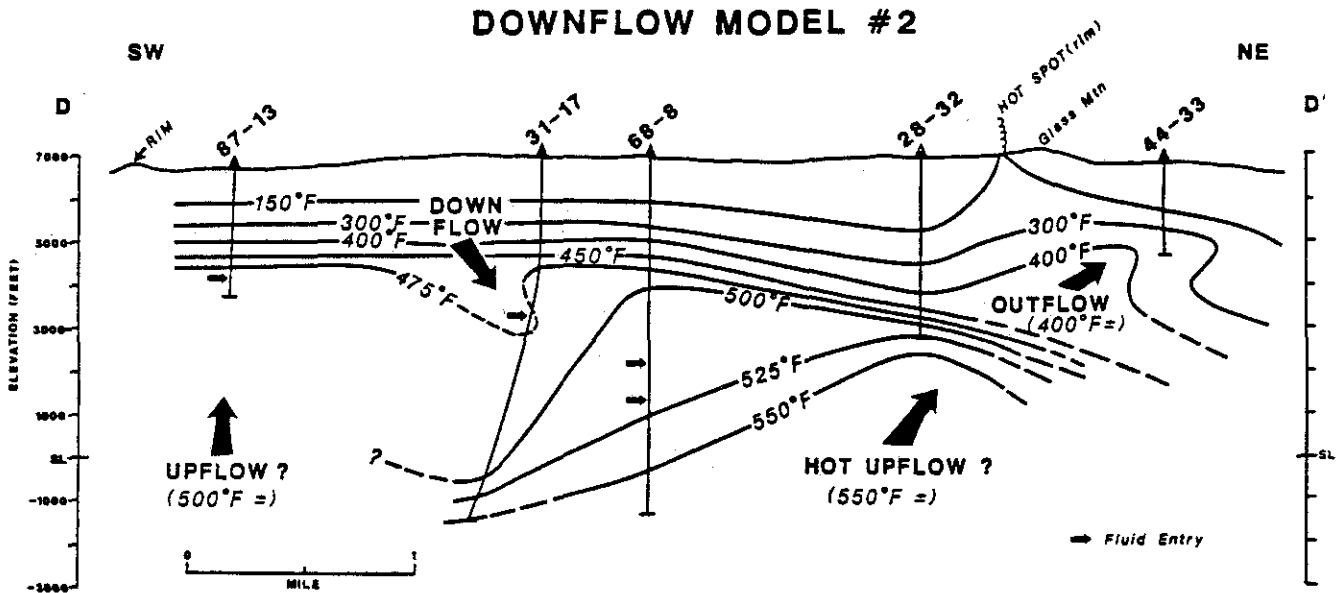


Figure 22. Reservoir downflow model #2 showing upflow near 87-13 and near Hot Spot.

An alternative model to reservoir downflow suggests that the temperature reversals are due to reservoir fluids with temperatures of about 485°F flowing laterally into hotter, conductively heated rock (Figure 23, Lateral Flow Model). As described in Downflow Model #1, resistivity, alteration, and permeability data suggest that a vigorous hydrothermal system exists in the southwest part of the conductance anomaly in the vicinity of 87-13. The Na-K-Ca chemical geothermometer suggests that the fluids produced from the well had a source temperature of about 485°F. Although fluid entry temperatures in 31-17 and 68-8 range from 475°F to at least 514°F, chemical geothermometers indicate that these fluids also had an original source temperature of about 480 - 485°F (Figure 19a). It is possible that reservoir fluids have leaked from the center of the system northeastward into hotter, less permeable rock, causing temperature reversals at fluid entry points.

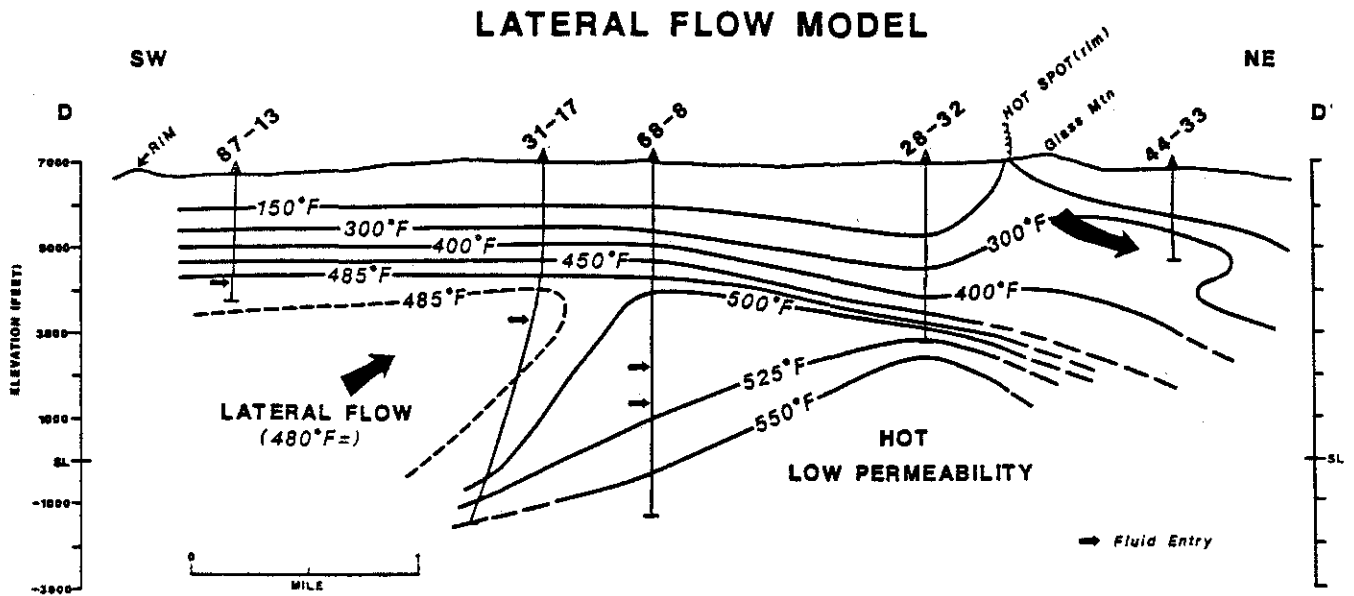


Figure 23. Lateral flow model.

One major inconsistency with the Lateral Flow Model is that the fluids produced from 87-13 are lower in chloride than from the other two wells (Figure 18b). If 87-13 is closer to upflow, then relatively higher salinities would be expected for the fluids. However, the short flow test and shallow depth of the well preclude any firm conclusions about the significance of the low fluid salinity. It is possible that both lateral flow of reservoir fluids and downflow of groundwater are occurring in the Glass Mountain geothermal system.

Deep drilling and additional flow testing will be required to differentiate between the proposed reservoir models. A deep well at the 87-13 site will answer whether high temperatures and permeability continue to depth. If so, wells with steam flow rates of 150,000-200,000 pounds per hour are likely in the area (Rosknecht, pers. comm.). To test the possibility of high temperature upflow near Glass Mountain, a deep well will eventually have to be drilled south or southeast of the Hot Spot. To determine whether downflow of cool water into the reservoir may occur, chemical monitoring and interference measurements during long-term flow testing will be needed.

LIST OF FIGURES AND PLATES

<u>Figures</u>	<u>Page</u>	
Figure 1	3	Location map of the Glass Mountain area.
Figure 2	5	Geologic cross sections through the Medicine Lake Volcano.
Figure 3	6	Residual Bouguer gravity contours and outline of shallow intrusive body.
Figure 4	7	Location of major fault zones.
Figure 5	7	Earthquake epicenter locations, September 1988-September 1989 (USGS data).
Figure 6	8	Two-dimensional MT interpretation with alteration zonation.
Figure 7	9	Contour map of TDEM Bostick resistivities at 1,500 feet depth.
Figure 8	10	Contour map of MT Bostick resistivities at 5,000 feet depth.
Figure 9	11	Total conductance integrated to a depth of 5,000 feet.
Figure 10	11	Location of major fault zones and conductance anomalies.
Figure 11	12	Geoelectric cross sections with contoured Bostick resistivities, Lines A-A' and B-B'.
Figure 12	13	Geoelectric cross sections with contoured Bostick resistivities, Lines C-C' and D-D'.
Figure 13	14	Interpreted temperature contours at 2,000 feet depth.
Figure 14	14	Interpreted temperature contours at 3,000 feet depth.
Figure 15	15	Temperature and alteration cross sections through the Medicine Lake Volcano.
Figure 16	16	Temperature vs elevation profiles from the wells 17a-6, 31-17, 68-8 and 87-13.
Figure 17	17	Total dissolved solids, total gas, and H ₂ S concentrations in reservoir fluids from Unocal geothermal fields.
Figure 18	18	Fluoride and chloride concentrations vs time for produced fluids from the Glass Mountain production wells.
Figure 19	19	Calculated chemical geothermometers vs time for produced fluids from the Glass Mountain production wells.
Figure 20	20	Interpreted temperature contours at 4,000 feet depth.
Figure 21	21	Reservoir downflow model #1 showing upflow near 87-13.
Figure 22	22	Reservoir downflow model #2 showing upflow near 87-13 and near Hot Spot.
Figure 23	23	Lateral flow model.
Figure Ia	27	Gravity interpretations: 2 1/2-D Models A-A' and B-B'.

REFERENCES

- Anderson, C.A., 1941, Volcanos of the Medicine Lake Highland, California, Univ. Calif. Berkeley Publ. Geol. Sci., 25, pp. 347-422.
- Carrier, D.L., 1987, Analysis of mineralogy and fluid inclusion data from Glass Mountain area temperature boreholes, Unocal, 40p.
- Carrier, D.L., 1989a, Hydrothermal alteration and well lithologies for Glass Mountain wells GMF68-8, GMF31-17 and GMF17A-6, Glass Mountain, CA., Unocal, UCA07.2701, 28p.
- Carrier, D.L. 1989b, Fluid inclusion studies on samples from Glass Mountain deep exploration wells, Unocal, UCA07.2702, 18p.
- Donnelly-Nolan, J.M., 1988, A magmatic model of Medicine Lake Volcano, California, J. Geophys. Res., vol. 93, pp. 4412-4420.
- Evans, J.R. and J.J. Zucca, 1988, Active high-resolution seismic tomography of compressional wave velocity and attenuation structure at Medicine Lake volcano, Northern California Cascade Range, J. Geophys. Res., vol. 93, pp. 15,016-15,036.
- Fuis, G.S., Zucca, J.J., Mooney, W.D., and Milkereit, B., 1987, A geologic interpretation of seismic-refraction results in northeastern California, GSA Bulletin, v. 98, pp. 53-65.
- Hausback, 1984, Surficial geology of the Medicine Lake Highland, Unocal, UCA05.1207, 20p.
- McDannel, A. and Bodell, J.M., 1985, Structural assessment of Medicine Lake Highland, Unocal, UCA05.1303, 10p.
- McNutt, S., 1989, Medicine Lake Highland September 1988 earthquake swarm, California Geology, pp. 51-52.
- Nordquist, G.A., 1986, Interpretation of the 1985 detailed TDEM survey in the Glass Mountain Unit Area, Unocal, 9p.
- Stark, M.A., 1985, New techniques for integration of TDEM and MT data: The number 5, Unocal, 10p.
- Thompson, K., 1981, Geology and petrology of the Bartle Quadrangle, northern California: B.A. Thesis, unpublished, Franklin and Marshall College, Pennsylvania, 86p.

Plates

- Plate 1 TDEM station locations and Bostick resistivities at 1,500 feet depth.
- Plate 2 MT station locations and Bostick resistivities at 5,000 feet depth.
- Plate 3 Total conductance integrated to a depth of 5,000 feet.
- Plate 4 Interpreted temperature contours at 4,000 feet depth and recommended temperature gradient and deep production test well locations.

Appendix I: Gravity Modelling

Gravity measurements over the Medicine Lake volcano delineate a symmetrical 16 mgal high which is interpreted to reflect a buried intrusive body (Figure 3). This is corroborated by 17a-6 and 31-17 which each encountered a granodiorite intrusion at a depth of about 8000 feet. The density structure beneath the volcano can be generalized into a higher density basement (2.75 gm/cc), consisting of plutonic and metamorphic rocks (Fuis et al., 1987), which are overlain by lower density volcanics (2.43 gm/cc) of the Cedarville series and Medicine Lake volcano. Using this structure, 2^{1/2}-D interpretations show the shallow intrusion at a depth of about 8000 feet is centered beneath the basin (Figure 3). The southeastern edge of the intrusion drops off abruptly near the wells 87-13 and 31-17, coincident with the Eastern Conductance Anomaly (Figure Ia).

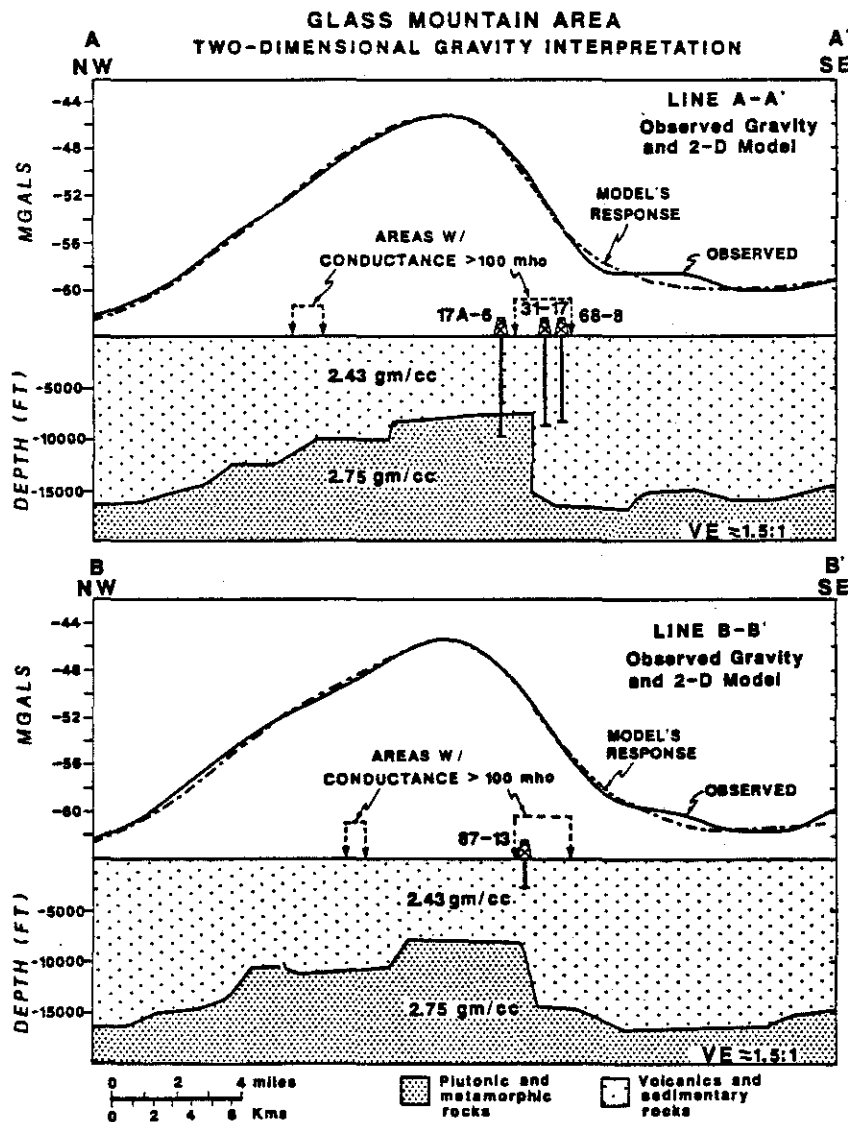


Figure Ia. Gravity interpretations: 2^{1/2}-D Models A-A' and B-B'. Location of section lines shown in Figure 3.

APPENDIX II. 87-13 X-RAY DIFFRACTION RESULTS

UURI

EARTH SCIENCE LABORATORY
391 CHIPETA WAY, SUITE C
SALT LAKE CITY, UTAH 84108-1295
TELEPHONE 801-524-3422

April 9, 1990

Randolph C. Thompson
Unocal Geothermal Division
3576 Unocal Place
P.O. Box 6854
Santa Rosa, California 95406

Dear Randy:

The lithologies in well 13 are similar to those previously studied in the "6", "8", and "17" series groups. However, unlike the other wells, no granodiorite or microgranodiorite is present in these samples from well 13.

Three major rock types are present. 1) Porphyritic to aphyric basalts and porphyritic basaltic andesites are commonly amygdular. 2) Coarser-grained rocks with abundant clino- and ortho- pyroxene are termed microdiabase, implying an intrusive origin for this rock type. Some of the microdibasases also contain minor amounts of biotite or hornblende. Phenocrysts in the coarser-grained diabasases are optically-textured. 3) Quartz latites or rhyodacites exhibit a variety of devitrification textures and probably were originally glassy.

In general, predominantly aphyric and amygdular basaltic andesite flows are present to 1200'. However, at 300' and 800', porphyritic dacite is also present. The dacites probably represent flows; they are flow-banded and contain altered phenocrysts of biotite and perthitically intergrown feldspars in glomeroporphyritic aggregates. Angular fragments of oxidized andesitic basalt in sample 1200' may represent cinders that are part of a volcanic cone at the base of the predominately basaltic flow section.

Samples from 1300' and 1400' are mostly porphyritic andesite and represent a flow or possibly, a shallow intrusive body. Sample 1460' is a mixture of many rock types and represents the contact

between the andesite and an underlying thick (1500'-1800') rhyodacite. The cuttings in 1460' include basalt and andesite flow rocks and rhyodacite flows or tuffs. Because such a variety of lithologies are present in 1460' and not in the overlying section, it is likely that this depth represents an erosional unconformity in the volcanic section.

The rhyodacite displays several different textures. Relict perlitic texture is evident at the top (1500') and near the bottom (at 1800'), coarser-grained rhyodacite is present. This crystallization pattern suggests that the rhyodacite was deposited as a flow or a flow-dome complex; it may have cooled quickly to a glass near the surface (now 1500') and more slowly near its center (now 1800'). Spherulitic devitrification is also common in the center of the rhyodacite body. At the base of the rhyodacite, sample 1890' contains many cuttings with an argillic matrix and rounded andesite clasts along with resorbed quartz phenocrysts. This rock is probably an intraformational mudflow with an ashy matrix. One chip in sample 1890' is of coarse-grained graphic intergrowths of feldspar and quartz which could have been derived from a granitic highland.

Below 2000', the rocks consist predominately of diabase that is gouged or mylonitic and highly altered.

Samples from 2000' to 2200' are mostly microdiabase which probably represents a brecciated intrusive body. Within the microdiabase are altered phenocrysts of a ferromagnesian mineral, probably hornblende but possibly biotite, which are completely altered (deuterically?) to smectite. Clinopyroxene phenocrysts subophitically enclose plagioclase laths in the coarse-grained diabase at 2100'.

Samples from 2300' to 2400' are mostly hornblende microdiabase. The presence of potassium feldspar at 2300' is somewhat problematical. There is certainly secondary adularia in this sample but it is also possible that some of the potassium feldspar is primary. In the latter case and considering the presence of hornblende, some of the lithologies at 2300' and 2400' may be termed porphyritic rhyodacite or quartz latite. Either way, samples 2300' and 2400' represent a different rock unit than from 2000' to 2200'.

Some of the microbreccia in microdiabase at 2300' and in andesite at 2370' may have been caused by hydrothermal brecciation; both samples contain rounded, hematitic fragments within a silicified matrix.

Sample 2450' is nearly identical to sample 2370', and sample 2400' is similar to sample 2300'. Samples 2370' and 2450' are vesicular basaltic andesites and both are intensely mineralized. This phenomenon may indicate that vesicular lithologies provide good permeability pathways for hydrothermal fluids.

Samples 2500' and 2560' contain two rock types; fine-grained, glassy andesite and coarser-grained diabase, both of which are probably just textural variations of the same rock. In sample 2500', both rock types are vesicular and the vesicles are filled with fluid inclusion-rich (hydrothermal) quartz and/or epidote. The glassy, aphyric andesite probably represents the cooled borders of the intrusive body. In chips of diabase at 2500', the clinopyroxene is coarse-grained and subophitically-encloses plagioclase.

Samples 2560' and 2600' are both intensely altered and mineralized, making the original rock type difficult to determine. However, these samples appear to be mostly microdiabase (flooded with secondary K-feldspar?). Sample 2560' also contains some porphyritic rhyodacite; large quartz and zoned plagioclase phenocrysts are present in a devitrified matrix of quartz and potassium feldspar. Some fragments of the rhyodacite appear sericitized. Relict shard and pumice texture is evident in some chips indicating that the rhyodacite is at least partially tuffaceous.

The rocks from well 13 are mineralogically zoned with depth. Argillic alteration predominates down to about 1000'. Smectite and zeolite-filled amygdules are common in the argillic zone, although some calcite-filled amygdules are present at 600' and 800'. X-ray diffraction analysis of the zeolite indicates that it is stilbite, a low-temperature, fibrous zeolite.

The first occurrence of hydrothermal veining (chlorite-smectite and quartz+pyrite) is at 1000'. The top of the propylitic zone is at 1100', where epidote first appears as a trace mineral in veins. Veins of intergrown quartz and calcite (+/- epidote and wairakite) in samples from 1100' to 1460' suggest that this may be a zone of extensive boiling. Dark green, highly birefringent smectite is common in this zone and is especially abundant in sample 1400'. All of the lithologies in sample 1460' are highly altered and it is likely that this interval is a lithologic contact that was permeable and promoted hydrothermal alteration.

In general, the rhyodacite flow from 1500' to 1890' is not as altered as the overlying and underlying rocks. Chips of andesitic or diabasic rocks within the rhyodacite interval commonly contain veins and much epidote but the rhyodacite itself is commonly just silicified. Some chips of the (originally glassier?) rhyodacite are also sericitized. X-ray diffraction analyses of the clay fractions from samples 1600', 1710' and 1890' indicate the presence of mixed-layer illite-smectite with about 10% smectite interlayers. Such illitic illite-smectites usually indicate temperatures up to 260°C (e.g. McDowell and Elders, 1980).

The microdiabases from 2000' to 2300' are brecciated and veined. In thin-section, sheared and microbrecciated or strained crystals in a dark chloritic matrix characterize mylonitic chips of diabase. Traces of talc in this interval may be associated with

the fault gouge. Actinolite is present in this interval both in veins with hydrothermal quartz and as a (deuteric?) alteration product of primary clinopyroxene and/or amphibole in the diabase.

Dark green smectite is also a common alteration mineral in the interval from 2000' to 2300'. At 2200', this smectite occurs in veins with actinolite and quartz. Therefore, it must be a high-temperature variety of smectite (e.g. Eberl, Whitney and Khoury, 1978). From the X-ray diffraction pattern, it is not possible to distinguish this clay as saponite (magnesium-rich smectite) or a smectite-rich chlorite-smectite. Nevertheless, it appears to be identical in XRD and in thin-section to the clay in the lower portions of well 8 (termed smectite) and well 17 (termed chlorite-smectite). In well 13, the smectite is mostly absent in the hottest part of the well (below 2300') and a very chloritic mixed-layer chlorite-smectite is the only clay mineral that persists to the bottom of the well.

From 2300' down to 2600', well-defined hydrothermal veins of prehnite+epidote and adularia+quartz (+/- epidote and actinolite) are common. Evidence for hydrothermal brecciation at 2370' and 2450' suggests that some boiling may have occurred locally. The presence of veins of anhydrite at 2370' and 2470' may indicate increased permeability due to hydrothermal brecciation and boiling.

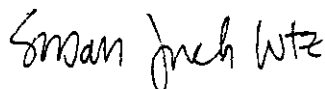
Potassium feldspar flooding of the diabase below 2300' is extensive. Because potassic alteration is typical of ascending and cooling solutions, the formation of K-feldspar in this zone may indicate the positioning of these rocks in or close to a major upflow zone (e.g. Giggenbach, 1984).

The secondary mineral assemblage from 2300' to 2600' is certainly indicative of deposition from high-temperature hydrothermal fluids. Epidote commonly forms above 240°C; prehnite above 250°C; and actinolite at temperatures greater than 250°C (e.g. Browne, 1978, 1984; Hulen and Nielson, 1986; Bird et al., 1984). Traces of grossular garnet in a vein with prehnite and epidote at 2560' may indicate temperatures above 300°C in this zone.

To conclude, the rocks in the lower portion of well 13 contain an abundance of unambiguous high-temperature hydrothermal minerals (particularly prehnite) in well-defined veins. The secondary (and perhaps metamorphic) mineral assemblage of biotite, actinolite and clinopyroxene which complicated interpretation of the hydrothermal alteration in the granodiorite of well 17 is not present.

At this point in your investigation, you should have the basis of a stratigraphic and structural framework for this area. If you don't and are willing to provide me with the thin-sections from, the depths of samples from, and the relative position of, wells 6, 8, 13 and 17, I would be very interested in working on this aspect of your investigation. Please contact me if you are interested in this proposal or if you have any questions concerning the X-ray diffraction or petrographic analyses of the rocks from well 13. Thanks for the opportunity to continue working on these interesting rocks.

Sincerely,



Susan Juch Lutz
Manager,
X-ray Diffraction Lab

References:

Bird, D.K., Schiffman, P., Elders, W.A., Williams, A.E., and McDowell, S.D., 1984, Calc-silicate mineralization in active geothermal systems: *Econ. Geol.*, v. 79, p. 671-695.

Browne, P.R.L., 1978, Hydrothermal alteration in active geothermal fields: *Ann. Rev. Earth Planet. Sci.*, v.6, p 229-250.

Browne, P.R.L., 1984, Lectures on geothermal geology and petrology: United Nations Univ., *Geoth. Training Prog.*, Rept. 1984-2, 92p.

Eberl, D., Whitney, G. and Khoury, H., 1978, Hydrothermal reactivity of smectite: *American Mineralogist*, v. 63, p. 401-409.

Giggenbach, W.F., 1984, Mass transfer in hydrothermal alteration systems- a conceptual approach: *Geochim. et Cosmochim. Acta*, v. 48, p. 2693-2711.

Hulen, J.B. and Nielson, D.L., 1986, Hydrothermal alteration in the Baca geothermal system, Redondo dome, Valles caldera, New Mexico: *J. Geophys. Res.*, v. 91, p. 1867-1886.

UNOCAL GEOTHERMAL DIVISION - RANDOLPH THOMPSON

WELL 13 MEDICINE LAKE		MINERALOGY, APPROX. WT.% <input checked="" type="checkbox"/> (or) RELATIVE ABUNDANCE <input type="checkbox"/>																	CLASS							
		CACISTOBALITE	QUARTZ	PLAGIOCLASE	K-FELDSPAR	CALCITE	ANHYDRITE	MAGNETITE	HEMATITE	PARITE	SPARRE-SCITILE LEUCOSINE UNIDY	CLINOPIROXENE	AMPHIBOLE	ACTINOLITE	EPIDOTE	PREHNITE	WAIKAKITE	STILBITE		TALC	SMECTITE	MIXED-LAYER MILONITE-SMECTITE	MIXED-LAYER ILLITE-CALCIC SMECTITE	MARK ABOVE BELOW DETECTION		
BULK + CLAY XRD SAMPLE NO.																										
160 BULK		TR	44				14	3											10					27	CLASS	
200 BULK	3	TR	61				20	TR											5					3		
CLAY																			100							
300 BULK	61		5	27			1	2									TR		4					-	X WITH GOETHITE	
400 BULK	4		29				10	2									4		43					8	X WITH GOETHITE	
CLAY																TR		100						COARSE-GRAINED ZEOLITE		
600 BULK	3		42		6		13	16									2		8					10		
CLAY																TR		100								
800 BULK		TR	52		3		18	1					4				TR		18						WITH OETHOPYROXENE WAS BIOTITE	
CLAY																		100								
1000 BULK		4	34		5		15	3	1				2						31	2				3		
1100 BULK		6	37		8		16	6	1	2	1		TR						9	5				9		
CLAY																		55	45							
1200 BULK		14	15	2?	10		13	12	1	6	TR					3			4	11				9		
CLAY																		18	82							
1300 BULK		5	27	4	12		10	1	2	7	8		1		TR				2	14				7		
1400 BULK		2	35		3		22	1	2	2	13				TR				1	11				8		
CLAY																		82	18							
1460 BULK		7	32	5	4		11	1	3	10	3		TR						8	9				7		
1500 BULK		5	30	12	32	2		2	TR	1	1		1		5				1	1	TR				7	
1600 BULK		4	26	19	33	2		3	1	2	1	1		2					2	2				2		
CLAY																			19	57	24					~ 10% SM IN M.L. 145M
1710 BULK		5	25	17	37	TR		2		2	2		2						1	2				5	CEMENT	
CLAY																			3	36	61					~ 10% SM IN M.L. 145M

MM = PREDOMINANT M = MAJOR m = MINOR Tr = TRACE ? = TENTATIVE IDENTIFICATION



SUMMARY OF X-RAY DIFFRACTION ANALYSIS
UNIVERSITY OF UTAH RESEARCH INSTITUTE, EARTH SCIENCE LABORATORY

S. Lutz
3-9-90

UNOCAL GEOTHERMAL DIVISION - RANDOLPH THOMPSON

WELL 13 MEDICINE LAKE BULK + CLAY XRD SAMPLE NO.		MINERALOGY, APPROX. WT.% <input checked="" type="checkbox"/> (or) RELATIVE ABUNDANCE <input type="checkbox"/>																								
		CRISTOBALITE	QUARTZ	PLAGIOCLASE	K-FELDSPAR	CALCITE	ANHYDRITE	MAGNETITE	HEMATITE	PYRITE	SPHENE	LEUCOCENE UNDIV.	CLAY	PIROXENE	AMPHIBOLE			ACTINOLITE	EPIDOTE	PREHNITE	WAIKAKITE	TALC	SMECTITE	MIXED-LAYER CHLORITE-SMECTITE	MIXED-LAYER ILLITE-SMECTITE	AMPHIBOLE BELOW DETECTION
1800	BULK	2	14	19	32	3		3		2	3	1		TR						9	4			8	CEMENT w/PYRITE	
1890	BULK CLAY	2	20	14	30	4		3		4	7			TR		4					9	3			-	
																				TR	46	+54				+ ~10% SM IN M.L. 1L/SM
2000	BULK		2	30	9	4		9		2	2	15	1	1					1	16	1			6		
2100	BULK CLAY		5	35	6	3		10	1	2	4	9		TR		1				10	4			10		
2200	BULK CLAY		2	45		3		15		2	3	10	TR	TR	TR					16	1			3		
2300	BULK		9	31	10	2		9		1	12	8	2	1	TR				1	9	5			-		
2370	BULK CLAY		10	26	11		2	5	1	1	13			14	5						11			1		
																					99					• ESSENTIALLY PURE CHLORITE
2400	BULK		6	45	11	2		10		1	4	7	1	1						8	1			3	CEMENT w/PYRITE	
2450	BULK CLAY		10	23	6		3	3	1	TR	15			16	6						11			6		
																					100					• ESSENTIALLY PURE CHLORITE
2500	BULK		5	40	11	1		4		3	10	6	2	8							10			-		
2560	BULK CLAY		7	31	7	1		7		3	13	3	1	12	1						11	2		-		
													5								91	+4				+ ~10% SM IN M.L. 1L/SM • VERY CHLORITIC
* 2600 (?)	BULK		10	26	5	1		4	1		17			15	4						9			8		
* dupl. of 2450'																										

MM = PREDOMINANT M = MAJOR m = MINOR Tr = TRACE ? = TENTATIVE IDENTIFICATION



SUMMARY OF X-RAY DIFFRACTION ANALYSIS
UNIVERSITY OF UTAH RESEARCH INSTITUTE, EARTH SCIENCE LABORATORY

S. Lutz
3-9-90

SAMPLE FOOTAGE	ROCK TYPES											
	BIOTACT ANDESITE	PO-PHYRIC ANDESITE	MICROPHITIC ANDESITE	RHYODIORITE + QZ	RHYODIORITE BASE	QZ LATTICE OR RHYOLITE	MICRO RHYOLITE	MIODACTE	HYPENOLITE	MICROBRACHYDORITE	DACITE	RHYOLITE ASH FLOW TUFF VOLCANIC CONGLOMERATE BOULDS MICROBRECCIA VEIN FRAGS.
160	aMM	m										
200	m	MM										'FLOW-BANDED
300								MM				'DEVITRIFIED, SOME PERLITIC TEX, ALTER. BIOTITE
400	aMM		TR									
600	aMM											
800								MM				'MUCH ALTERED BIOTITE, SOME CPX + OPX, + FLOW-BANDED
1000	aM	m	m								m	
1100	aMM									TR	m	
1200	aMM										m	ANGULAR FRAGS. + HEM. = CINDERS? SPHERULITIC
1300		aMM		m							m	
1400	m	MM									m	m
1460	aM	M		M				m		m	m	'DEVITRIFIED ALSO RELECT SHARD TEX. RELECT PERLITIC TEX. SPHERULITIC DEVITR. EPIDOTE
1500			TR	MM							TR	TR
1600	aM		m	M						TR	TR	
1710			m	MM								
1800	m		m	M							TR	
1890	aM			M		TR?				M		
2000			MM								M	m
2100	TR		MM	TR							M	m
2200			MM								m	m
2300			MM								m	m
2370	aMM										m	M
2400			MM								m	m
2450	aMM											M
2500	aM		m								M	m
2560	m		M		m				m?		m	m
* 2600	m		M								m	m
a = AMYGDALAR												
* dupl of 2450'												

GRAPHIC F
BIOTITE

MORE XL
THAN 300

MIXTURE
OF ROCKS

ROUND
ANDESITE
CLASTS IN
CLAYEN
MATRIX

BRACIA?

WELL 13
MEDICINE LAKE

ROCK TYPES OBSERVED DURING
RECONNAISSANCE PETROGRAPHY

SAMPLE FOOTAGE	VEINLETS & VEINLET FRAGMENTS														
	QTZ	QTZ + PY	QTZ + CC	ANH ± CC	CALCITE	CHL ± CC	SMECTITE	WAIR ± CC	EP ± CC	EPIDOTE	PREHNITE		KF ± QTZ	ACT ± QTZ	TALC
160															MAGN → HEM, GLASSY
200															SOME SMECTITE
300															BIO → SMECT
400															SMECT, ZEPHITES IN AMYGDULES
600															MAGN → HEM, CC - FILLED AMYGDULES, HEM
800				✓											ZEPHITE, CC, SMECT - FILLED AMYGDULES
1000		✓		✓	✓										FIRST PY, CHL
1100	✓	✓ _{leuc}	✓	✓	✓				✓ _{ACT}						FIRST EP, BOILING ASSEMBLAGE?
1200	✓	✓	✓		✓			✓ _{CC}							MAGN → HEM, QTZ + WAIR IN AMYGDULES
1300	✓	✓	✓	✓	✓			✓	✓	✓					EP + CHL, PY, LEUCOKENE
1400		✓	✓					✓							MUCH DR. GREEN SMECTITE, TR. CHANADO NY
1460	✓		✓	✓			✓ _{ACT}		✓						PLAG → EP + CHL, LEUCOKENE
1500	✓			✓			✓ _{ACT}								SILICIFIED, BIG WAIR VEINS
1600	✓	✓	✓	✓					✓						EP IN MICRODIABASE, SILICIFIED RHODACITE
1710	✓								✓						"
1800	✓	✓							✓ _{CHL}						" LEUCOKENE
1890	✓	✓		✓				✓ _{EP}	✓						SOME SERICITE
2000		✓			✓				✓ _{ACT}		✓ _{EP}	✓			FIRST ACTINOLITE, TALC, MUCH SMECTITE
2100	✓						✓ _{ACT}	✓	✓			✓			
2200				✓	✓			✓	✓	✓		✓	✓ _{ACT}		ACT + QTZ + SMECTITE, FIRST PREHNITE
2300	✓ _{CHL}	✓	✓ _{EP}						✓ _{ACT}	✓	✓	✓	✓		BOILING ASSEMBLAGE? KF FLOODING?
2370			✓ _{EP}	✓			✓	✓	✓ _{EP}	✓ _{EP}	✓ _{EP}	✓	✓		INTENSELY MINERALIZED, HEM, PARHEDRONS IN
2400	✓								✓ _{ACT}	✓ _{ACT}	✓ _{EP}	✓ _{EP}	✓		KF + QTZ + ACT + EP VEINS, KF FLOODING
2450			✓ _{EP}	✓					✓ _{ACT}	✓ _{EP}	✓	✓	✓ _{EP}		MINERALIZED, HEM, LEUCOKENE
2500		✓		✓					✓ _{ACT}	✓ _{EP}	✓	✓	✓ _{EP}		KF FLOODING
2560					✓				✓ _{ACT}	✓ _{EP}		✓			LOTS OF ACTINOLITE + CHL IN DIABASE, SOME SERICITE
* 2600	✓				✓				✓ _{ACT}	✓ _{EP}	✓ _{PREH}				HEM + LEUCOKENE, KF FLOODING, MINERALIZED
* dupl of 2450'															

WELL 13
MEDICINE LAKE

VEINLETS OBSERVED DURING
RECONNAISSANCE PETROGRAPHY

APPENDIX III. FLUID CHEMISTRY

<u>SAMPLE</u>	<u>DATE</u>	<u>TDS</u> (ppm)	<u>GAS/STM</u> (WT %)	<u>H₂S</u> (ppm)	<u>F</u> (ppm)	<u>Cl</u> (ppm)	<u>TNKC</u> (°F)	<u>TOTZ</u> (°F)
31-17								
31-17-II-1	10-18-88	3539			11.62	1706	448.4	529.2
31-17-II-2	10-18-88	3524	0.019	31	10.89	1699	446.2	536.4
31-17-II-3	10-18-88	3404			8.713	1619	449.1	534.2
31-17-II-4	10-19-88	3262			8.713	1568	448.7	527.0
31-17-II-5	10-19-88	3335			8.277	1568	450.3	535.8
31-17-II-6	10-19-88	3345			8.277	1554	453.4	537.7
31-17-II-7	10-19-88	3196	0.077	20	7.983	1531	449.9	523.4
31-17-II-8	10-20-88	3197			7.697	1518	451.7	525.7
31-17-II-9	10-20-88	3230			7.116	1518	442.4	529.8
31-17-II-10	10-20-88	3140			7.043	1518	454.3	518.3
31-17-II-11	10-20-88	3190			9.439	1489	455.8	516.8
31-17-II-12	10-21-88	3214			6.172	1488	458.7	521.4
31-17-II-13	10-21-88	3115			6.099	1489	455.6	513.7
31-17-II-14	10-21-88	3213			6.244	1510	460.5	515.0
31-17-II-15	10-21-88	3145			6.172	1474	459.4	514.0
31-17-II-16	10-22-88	3087			6.027	1474	456.8	510.7
31-17-II-17	10-22-88	3118			5.809	1474	459.5	512.8
31-17-II-18	10-22-88	3075			5.809	1474	459.8	506.5
31-17-II-19	10-22-88	3046			5.809	1475	458.0	504.1
31-17-II-20	10-23-88	3065			5.519	1474	460.6	503.5
31-17-II-21	10-23-88	3168			5.446	1467	463.1	516.8
31-17-II-23	10-23-88	3133	0.021	84	5.082	1459	463.5	511.9
31-17-II-24	10-24-88	3100			5.083	1445	465.0	505.9
31-17-II-25	10-24-88	3132			4.792	1467	465.1	508.6
31-17-II-26	10-24-88	3024			5.083	1438	464.5	498.8
31-17-II-27	10-25-88	3032			4.575	1430	464.5	499.1
31-17-II-28	10-25-88	3048			4.792	1430	465.3	499.4
31-17-II-29	10-25-88	3079			4.720	1438	466.7	502.0
31-17-II-30	10-26-88	3053			4.502	1438	467.0	500.5
31-17-II-31	10-26-88	3054			4.212	1445	466.3	501.7
31-17-II-32	10-26-88	3083			4.429	1445	468.2	500.2
31-17-II-33	10-27-88	3088			4.357	1445	468.7	499.4
31-17-II-34	10-27-88	3088			3.994	1445	469.4	499.7
31-17-II-35	10-27-88	3033			4.066	1445	469.1	494.9
31-17-II-36	10-28-88	3076			4.139	1445	471.3	497.3
31-17-II-37	10-28-88	3073			3.848	1445	471.8	497.0
31-17-II-38	10-28-88	3071			3.921	1445	471.6	496.7
31-17-II-39	10-29-88	3070			3.848	1445	470.5	499.4
31-17-II-40	10-29-88	3040			3.631	1438	471.3	495.2
31-17-II-41	10-29-88	2976			3.558	1394	471.2	491.7
31-17-II-42	10-30-88	2980			3.849	1387	471.3	493.1
3117-1	081489	2983			3.923	1421	468.8	492.8
3117-1A	081489	2986			3.676	1437	469.5	492.5
3117-A	890814		0.080	40				
3117-1B	890814	3005	0.075	48	3.688	1442	470.1	493.1
3117-1C	081489	3021			3.481	1442	470.8	493.5
3117-2	081589	2986			3.719	1421	472.7	494.1

APPENDIX III. FLUID CHEMISTRY (Continued)

<u>SAMPLE</u>	<u>DATE</u>	<u>TDS</u> <u>(ppm)</u>	<u>GAS/STM</u> <u>(WT %)</u>	<u>H₂S</u> <u>(ppm)</u>	<u>F</u> <u>(ppm)</u>	<u>Cl</u> <u>(ppm)</u>	<u>TNKC</u> <u>(°F)</u>	<u>TQTZ</u> <u>(°F)</u>
3117-2A	081589	2969			3.389	1424	474.2	490.7
3117-3	081689	3012			3.058	1439	475.0	494.0
3117-4	890817	2956	0.096	64	2.834	1421	476.5	489.5
3117-B	890817		0.100	49				
3117-5	081889	2971			2.797	1438	479.9	490.6
3117-6	081989	2949			2.695	1400	475.8	490.6
3117-7	082189	2955			2.605	1405	477.1	491.2
3117-8	890824	2962	0.034	48	4.070	1395	480.4	490.0
3117-C	890824		0.070	45				
3117-9	082589	2975			2.716	1411	480.4	491.3
3117-10	082689	2968			2.692	1395	480.8	495.3
3117-11	082789	2947			2.692	1378	480.6	494.9
3117-12	890828	2907	0.075	48	2.524	1376	479.8	492.9
3117-D	890828		0.070	49				
3117-T	890828		0.071	43				
68-8								
68-8-III-1	9-17-88	2113			1.170	988.	454.9	425.1
68-8-III-11	9-17-88	2922			1.503	1333	480.4	502.7
68-8-III-14	9-17-88	2846			1.601	1326	479.8	489.3
68-8-III-16	9-18-88	2819			1.369	1293	484.9	499.0
68-8-III-18	9-18-88	2933	0.041		1.371	1367	489.0	504.0
68-8-III-19	9-18-88	2986			1.471	1427	487.2	505.7
68-8-III-2	9-17-88	3069			1.838	1475	462.2	474.3
68-8-III-6	9-17-88	3087			1.668	1464	465.8	484.2
68-8-III-8	9-17-88	2824			1.471	1295	477.1	498.4
68-8-IV-1	9-22-88	3191			1.576	1499	479.7	509.8
68-8-IV-10	9-25-88	2673	0.037		1.471	1247	492.0	483.8
68-8-IV-4	9-22-88	3076			1.628	1493	483.1	490.7
68-8-IV-5	9-23-88	3059			1.669	1432	486.3	505.5
68-8-IV-7	9-23-88	3019			1.202	1416	487.8	510.0
68-8-IV-8	9-24-88	2919	0.014		1.601	1391	486.1	483.6
68-8-IV-9	9-24-88	2977	0.055		1.443	1394	491.0	498.1
68-8-1	090789	3588			7.226	1621	434.7	466.2
68-8-1A	090789	3733			7.697	1675	436.2	484.5
68-8-2	090889	3797			9.912	1721	438.0	497.9
68-8-2A	090889	3588			7.659	1640	436.0	482.5
68-8-3	090989	3726			9.870	1723	439.5	505.5
68-8-3A	090989	3887			11.67	1768	441.6	520.4
68-8-3B	090989	3905			10.77	1759	441.7	525.0
68-8-4	091089	3930			12.50	1795	444.7	530.4
68-8-4A	091089	3827			10.72	1750	444.0	526.2
68-8-4B	091089	3969			12.95	1840	445.0	534.3
68-8-5	091189	3945			11.62	1842	445.5	537.4
68-8-6	091589	4001			11.39	1968	465.0	569.1

APPENDIX III. FLUID CHEMISTRY (Continued)

<u>SAMPLE</u>	<u>DATE</u>	<u>TDS</u> <u>(ppm)</u>	<u>GAS/STM</u> <u>(WT %)</u>	<u>H₂S</u> <u>(ppm)</u>	<u>F</u> <u>(ppm)</u>	<u>Cl</u> <u>(ppm)</u>	<u>TNKC</u> <u>(°F)</u>	<u>TOTZ</u> <u>(°F)</u>
68-8-7	091889	3932			8.069	1860	458.2	569.2
68-8-8	890920	3757	0.138	48	6.682	1785	460.6	557.7
68-8-A	890920		0.150	50				
68-8-9	890921	3732			6.339	1792	461.9	552.8
68-8-10	890923	3677			5.361	1776	464.2	549.4
68-8-11	890924	3597			4.906	1713	465.5	548.4
68-8-12	890925	3544			5.398	1669	467.2	546.1
68-8-13	092689	3487			5.419	1650	468.1	540.1
68-8-14	092789	3473			5.206	1653	468.4	539.6
68-8-15	092889	3475			5.357	1632	469.3	546.6
68-8-16	092978	3458			5.275	1632	470.0	544.0
68-8-17	093089	3416			5.330	1615	471.0	540.1
68-8-18	100189	3388			4.898	1608	472.6	536.0
68-8-19	100289	3398			4.984	1601	471.1	546.1
68-8-20	891004	3314			5.118	1568	473.7	534.3
68-8-21	891005	3314			5.089	1567	475.5	534.6
68-8-22	891006	3281			4.856	1560	475.5	531.2
68-8-23	891009	3201	0.140	53	4.697	1520	477.0	527.1
68-8-B	891009		0.150	59				
68-8-24	891010	3310			5.087	1558	248.7	538.9
68-8-25	891011	3215	0.150	51	4.690	1518	480.1	527.5
68-8-26	891012	3252			4.804	1537	481.4	530.3
68-8-27	981013	3261			4.404	1537	482.4	531.3
68-8-28	891014	3181			4.865	1499	482.8	524.1
68-8-29	101689	3110			4.453	1474	482.8	522.0
68-8-30	891018	2962			4.271	1397	476.9	508.1
68-8-31	891019	3060			4.658	1432	251.0	517.4
68-8-32	891020	3094	0.150	59	4.588	1462	480.8	518.2
68-8-33	891024	3093			3.887	1446	484.5	518.4
68-8-34	891025	3083			3.720	1461	483.3	514.7
68-8-35	891027	3082			3.550	1455	484.5	517.0
68-8-36	891028	3091			3.762	1447	484.8	520.7
68-8-37	891029	3094			3.834	1438	485.3	521.0
68-8-38	891030	3058			3.532	1421	483.0	516.5
68-8-E	891031		0.150	64				
87-13								
87-13-4	891106	2316			0.956	940.	482.5	519.6
87-13-4A	891106	2287	0.859	142	0.932	923.	483.3	516.4
87-13-4C	891106	2335	0.121	34	0.883	954.	485.0	519.2